ELSEVIER

Contents lists available at ScienceDirect

Acta Biomaterialia

journal homepage: www.elsevier.com/locate/actbio



Full length article

Biodegradable Zn-Cu alloys show antibacterial activity against MRSA bone infection by inhibiting pathogen adhesion and biofilm formation



Xinhua Qu^{a,c,1}, Hongtao Yang^{b,e,1}, Bo Jia^{a,f,1}, Zhifeng Yu^a, Yufeng Zheng^{b,d,*}, Kerong Dai^{a,**}

- ^a Shanghai Key Laboratory of Orthopaedic Implants, Department of Orthopaedic Surgery, Shanghai Ninth People's Hospital, Shanghai Jiaotong University, School of Medicine, Shanghai 200011, China
- ^b Department of Materials Science and Engineering, College of Engineering, Peking University, Beijing 100871, China
- Department of Bone and Joint Surgery, Renji Hospital, School of Medicine, Shanghai Jiao Tong University, Shanghai 200127, China
- d International Research Organization for Advanced Science and Technology, Kumamoto University, 2-39-1 Kurokami, Chuo-Ku, Kumamoto 860-8555, Japan
- e Department of Materials Science and Engineering, The Ohio State University, Columbus, OH 43210, United States
- Department of Orthopedics, Shanghai General Hospital, Shanghai Jiao Tong University School of Medicine, Shanghai 200080, P. R. China

ARTICLE INFO

Article history: Received 14 May 2020 Revised 20 September 2020 Accepted 22 September 2020 Available online 29 September 2020

Keywords:
Bone and joint infection
Biodegradable metal
Zn-Cu alloy
Antibacterial activity
Osteomyelitis

ABSTRACT

Bone and joint-related infections remain the primary and most critical complications of orthopedic surgery. We have innovatively prepared Zn-Cu alloys to achieve outstanding material and antibacterial properties. In this study, we systematically assessed the material properties and antibacterial activity of these Zn-Cu alloys. Our results showed that the Zn-2Cu alloy had the best mechanical properties, biocompatibility, and osteogenic properties. Findings of microbial cultures, CLSM, SEM, and TEM indicated that Zn-2Cu alloy can inhibit both coagulase-positive and coagulase-negative staphylococci, as well as antibiotic-resistant strains (MRSA and MRSE), by preventing the bacteria adhesion and the biofilm formation. Zn-2Cu alloy could broadly affect the expression of MRSA genes associated with adhesion, autolysis, biofilm formation, virulence, and drug resistance. A rat femur intramedullary nail infection-prevention model was established and the Zn-2Cu alloy-treated group showed significant antibacterial activity against MRSA and reduced the inflammatory toxic side-effects and infection-related bone loss. Collectively, our results indicate the potential utility of Zn-Cu alloy implants with 2 wt% Cu in treating orthopedic infections.

Statement of significance: Osteomyelitis is a serious complication of orthopedic surgeries. Wide use of antibiotics contributes to the appearance of multi-drug resistant strains like methicillin-resistant staphylococcus aureus (MRSA). Alternatively, anti-osteomyelitis implants with broad-spectrum antibacterial properties can be favorable. Here, the antibacterial performance of biodegradable Zn-Cu alloys was evaluated with four different bacteria strains including antibiotic-resistant strains (MRSA and MRSE). Zn-Cu alloys exert excellent bacterial killing capability in all strains. In a rat femur infection model, the alloy showed significant antibacterial activity against MRSA and reduced inflammatory toxic side-effects as well as infection-related bone loss. The antibacterial property of Zn-2Cu alloy was associated with inhibition of gene expression related to wall synthesis, adhesion, colonization, biofilm formation, autolysis, and secretion of virulence factors in MRSA.

© 2020 Acta Materialia Inc. Published by Elsevier Ltd. All rights reserved.

E-mail addresses: yfzheng@pku.edu.cn (Y. Zheng), krdai@163.com (K. Dai).

1. Introduction

Despite advances in medical and surgical therapies, bone- and joint-related infections such as osteomyelitis and implant infections are still the primary and most critical complications of orthopedic surgery [1]. The postoperative infection rate remains high, especially for patients at a high risk of infection: 8-10% in open long bone fractures [2,3], 8.8% in primary lumbar fusions [4], 12.2% in revision lumbar fusions [4], 24.8% in revision of periprosthetic joint infection [5].

^{*} Corresponding author at: Department of Materials Science and Engineering, College of Engineering, Peking University, Beijing 100871, China.

^{**} Corresponding author at: Shanghai Key Laboratory of Orthopaedic Implants, Department of Orthopaedics, Ninth People's Hospital, Shanghai Jiao Tong University, School of Medicine, 639 Zhizaoju Road, Shanghai, 200011, China.

 $^{^{\}rm 1}\,$ Dr. Xinhua Qu, Dr. Hongtao Yang and Bo Jia, contributed equally to this study.

Internal implants are necessary for most orthopedic surgeries. However, it is easy to contract infection from internal implants in orthopedic surgery. The interface between the implant and bone tissue is known to be an immunodeficient fibrotic inflammation area (an area of host immunosuppression and reduced antiinfection ability), where bacteria can easily adhere, colonize, and cause infection [6]. Once bacteria adhere to the implant surface, they secrete bacterial adhesins and various protein-polysaccharide complexes, adhering more firmly and forming a bacterial biofilm that further resists host defenses and antibiotics [7,8]. Although first and second-generation cephalosporins are routinely administered perioperatively in orthopedic surgery, they are ineffective against multi-drug resistant strains such as methicillin-resistant Staphylococcus aureus (MRSA) [9]. Additionally, a sizeable proportion of orthopedic postoperative implant infections, especially in susceptible patients, are usually opportunistic and not acute. Generally, onset of infections may occur in six months or even years. A high risk of infection remains as long as the implants are present.

In general, the mechanism of implant infection is that the free bacteria contact and adhere to the material surface to form a bacterial biofilm that is difficult to remove [6]. The best way to prevent implant-related infection is "No implants," where the disappearance of the platform or surface will deprive the bacteria of necessary living space. Biodegradable anti-microbial implants, which can prevent infection from the source, might thus be the best solution to prevent orthopedic postoperative infections. The promising candidate materials should meet at least the following criteria: 1) acceptable cytocompatibility; 2) slow initial biodegradation rates, and maintaining sufficient mechanical support for at least six months; 3) continuous antibacterial capability to prevent the adhesion of bacteria and biofilm formation; and 4) complete degradation after fulfilling their internal-fixation and anti-bacterial functions.

Mg-based biodegradable materials have been considered as promising platforms for developing orthopedic implants with antibacterial properties. However, their fast degradation and inadequate mechanical performance limit their further applications. Our previous work showed that Cu ion-mediated anti-bacterial Mgalloy systems degraded too fast, generating large amounts of gas and losing their mechanical integrity at an early stage [10,11]. Another study reported that Mg-Cu alloys degraded almost completely in Hanks' solution within a week [12]. Moreover, the antibacterial coatings on Mg alloys were easily damaged and detached from the implants, exposing the underlying matrix and causing localized corrosion [13-16]. Compared to Mg-based materials, the degradation behavior of Zn-based materials is more desirable [17], and no gas-related issue has been observed with Zn-based materials yet [18–21]. Therefore, biodegradable Zn alloys have recently been reported as alternative candidates for orthopedic implants [22]. Among them, the Zn-Cu alloy system was developed and demonstrated satisfying mechanical performance, appropriate degradation behavior, and acceptable cytocompatibility in vitro and in vivo [23]. Cu has a broad spectrum of antibacterial properties, and has been widely used as an antibacterial element in orthopedics [24,25]. Cu presents anti-inflammatory, antimicrobial, and anti-proliferative properties in both its metallic form and chemical compound form [26,27]. Cu ion has been successfully incorporated into orthopedic and oral implant materials such as titanium (Ti), stainless steel (SS), and Mg alloys to equip them with bacteria-killing properties [28–34]. However, only two studies have examined the antibacterial activity of Zn-Cu alloys against S. aureus in vitro till now [23,35]. Further, information regarding the capability of Zn-Cu alloys against different bacterial species and the underlying anti-bacterial mechanisms is limited. More importantly, in vivo studies are necessary to evaluate the biosafety and antibacterial effectiveness of Zn-Cu alloys.

In this study, *in vitro* and *in vivo* studies were conducted systematically on biodegradable Zn–Cu alloys. MC3T3–K cells were used to evaluate the influence of Zn–Cu alloys on cytocompatibility and osteogenic differentiation. Four bacterial strains including two coagulase-positive staphylococci (MRSA and *S. aureus*) and two coagulase-negative staphylococci (MRSE and *S. epidermidis*) were used to investigate the *in vitro* antibacterial property of Zn–Cu alloys. A rat femur model infected with MRSA was established to study the *in vivo* antibacterial performance of Zn–Cu alloys. Finally, the mechanism underlying the antibacterial performance of Zn–Cu alloys was further revealed at the genetic level.

2. Experimental section

Figure S1 shows a flowchart of the study.

2.1. Pure Zn and Zn-Cu alloy preparation

The experimental Zn-Cu alloys were prepared from high-purity Zn (99.99%) and Cu (99.9%) bulk raw materials at different mass percentages. They were ultimately grouped into four kinds of experimental materials based on Cu mass ratios of 0 wt%, 0.5 wt%, 1 wt%, and 2 wt%, referred to as pure Zn, Zn-0.5Cu, Zn-1Cu, and Zn-2Cu, respectively. Prior to extrusion, pure Zn and Zn-Cu binary Zn alloy ingots were homogenized at 350°C for 48 h and guenched with water. Thereafter, before extrusion, they were kept at 260°C for 2 h, and then extruded at a ratio of 36 and a speed of 1 mm/s. The final diameter of the extruded bar was 10 mm. The experimental pure Zn and Zn-Cu alloys were cut into discs (Φ 10 \times 1 mm) and cylinders (Φ 1.8 \times 10 mm). Each sample was mechanically polished to a mesh of 2000, followed by ultrasonic cleaning in acetone and ethanol, and drying at room temperature. Samples were sterilized using ethylene oxide (provided by the Disinfection Supply Center of the Ninth People's Hospital affiliated to Shanghai Jiao Tong University School of Medicine) before performing cytotoxicity and animal experiments.

2.2. Microstructure and mechanical properties

The samples were ground to a reflective surface using a 0.5 μ m diamond polishing paste, rinsed with deionized water, and then blown dry. After immersion in 4% nitric acid alcohol solution for 5–10 s, they were rinsed using absolute ethanol, and after drying, their microstructure was observed using a metallurgical microscope (Olympus BX51M). The microstructural organization of the pure Zn and Zn–Cu alloys was determined with an X-ray diffractometer (XRD, Rigaku DMAX 2400, Japan) using CuK α radiation with a scanning range of 20–90° and a scanning speed of 4°/min.

The mechanical properties of the pure Zn and Zn–Cu alloys were evaluated by mechanical tests. The mechanical properties of the experimental pure Zn and Zn–Cu alloys were tested using Instron 5969 universal material testing machine (Instron-5969, Instron, USA). The sample had a gauge length of 25 mm, a strain rate of $1\times 10^{-4}/\rm s$, and was stretched at room temperature. Five parallel samples were tested for statistical analysis. The yield strength was defined as the corresponding stress at which the sample gauge length was plastically deformed by 0.2%.

2.3. Immersion test

Immersion tests were carried out in SBF solution at 37°C for 30 days. The pH value of the solution was recorded using a pH meter (Mettler FiveEasy pH FE20K) at different time points during wetting. After removing the products of corrosion, the weight loss of the sample was measured on an electronic balance (XS105,

Mettler Toledo) with a measurement sensitivity of 0.1 mg. On average, five measurements were performed for each group. The *in vitro* corrosion rate was calculated according to the following formula: $C = \Delta m/\rho At$, where C is the corrosion rate in mm/year, Δm is the weight loss, ρ is the density of the material, A is the surface area, and t is the implantation time.

2.4. Preparation of Zn-Cu alloy extracts

Extracts were prepared according to ISO 10993 standards. The experimental materials were immersed in the prepared α -MEM cell culture medium and transferred to a 37°C, 5% CO₂ environment at a specific surface area ratio of 1.25 mL/cm². Extracts were collected after 24 h, filtered through a sterile filter, stored at 4°C, and used within 3 days.

2.5. In vitro cell experiments

MC3T3-Kusao (hereafter referred to as MC3T3-K) cells were used to determine the biosafety and osteogenic induction of experimental pure Zn and Zn–Cu alloys. This cell line is an osteogenic precursor cell line and was a gift from Professor Hong Zhou of the University of Sydney, Australia.

2.5.1. Cell proliferation and viability assays

MC3T3-K cell proliferation and cytotoxicity were analyzed using the Cell Counting Kit-8 (CCK-8, Dojindo Molecular Technology, Japan) reagent. After counting the cultured cells, the cells were seeded in a 96-well plate (100 μ L, 2 × 10⁴ cells/mL) and incubated for 2–4 h in a cell culture incubator (37°C, 5% CO₂, saturated humidity) for adhesion. The cell mixture was mixed with pure Zn and Zn–Cu alloy extracts, and five sub-wells were inoculated in each group. Measurements were performed at 24, 48, and 72 h. To further verify the effect of Zn-based biodegradable metal extracts on the activity of MC3T3-K cells, Live/Dead cell staining and cytoskeletal staining (tetramethylrhodamine isothiocyanate-labeled primary antibody, phalloidin cytoskeletal labeling, and DAPI nuclear counterstaining) were performed on the cells. Cell survival and spreading were observed using a laser confocal microscope.

2.5.2. Cell osteogenic differentiation assays

After counting the MC3T3-K cells, the cells were seeded in a 6-well plate at 2 mL per well and incubated for 2-4 h in a cell culture incubator (37°C, 5% CO₂, saturated humidity) for adhesion. Pure Zn and Zn-Cu alloy extracts were added for co-culture, and three sub-wells were inoculated in each group. The culture medium was changed every other day. The status of the cells was observed every day. After the MC3T3-K cells reached 80% confluence, the medium was replaced with prepared osteogenic induction medium, which was changed every other day. After inducing differentiation for 10 days, the culture was ended, the osteogenic induction solution was discarded, the cells were washed gently with PBS three times, and then, the alkaline phosphatase activity of the MC3T3-K cells was quantitatively analyzed according to the protocol of the ALP quantitative assay kit (Nanjing Jiancheng). Additionally, MC3T3-K cells from each treatment group were stained and photographed according to the ALP staining protocol (Shanghai Honggiao).

2.5.3. Measurement of osteogenesis-related gene expression

Real-time reverse transcription quantitative PCR (RT-PCR) was used to measure the expression of osteogenesis-related genes. The expression of MC3T3-K cell marker genes (ALP, OCN, Col I, and Runx-2) was measured. After counting the MC3T3-K cells, the cells were seeded in a 6-well plate at 2 mL per well and incubated for

2-4 h in a cell culture incubator (37°C, 5% CO₂, saturated humidity) for adhesion. Pure Zn and Zn-Cu alloy extracts were added for co-culture and three sub-wells were inoculated in each group. The culture medium was changed every other day. Prepared osteogenic induction diluent was used to prepare 1-fold and 2-fold dilutions of the experimental material extracts. The status of the cells was observed every day. After the MC3T3-K cells reached 80% confluence, the medium was replaced with the prepared dilutions, and the dilutions were changed every other day. After 10 d of induction culture, total RNA was extracted using the RNeasy mini kit (Qiagen) per the manufacturer's instructions. RT-PCR was performed using the extracted total RNA to determine the mRNA expression of osteoblast marker genes (ALP, OCN, RunX-2, and ColI), with β actin as the internal reference. Primer sequences are shown in Table S1. A reverse transcription reagent kit (SuperScriptTM III Reverse Transcriptase) was used to reverse-transcribe 1 mg of RNA, SYBR Premix Ex Taq II (2 \times) was used as the PCR reagent, and RT-PCR was performed on the ABI 7500 Fast machine (Applied Biosystems, Courtaboeuf, France). The reaction conditions were as follows: 95° C for 30 s; 95° C for 5 s + 60° C for 40 s, 40 cycles; melting curve, 95° C 15 s + 60° C 1 min + 95° C 15 s. The results were calculated using the $2^{-\Delta\Delta Ct}$ method. $\Delta\Delta Ct =$ (the average Ct value of the gene to be tested - the average Ct value of the internal reference gene to be tested) - (the average Ct value of the target gene of the control - the average Ct value of the internal reference gene of the control).

2.6. In vitro anti-infection experiments

2.6.1. Bacterial isolation and culture

In this part of the study, four strains were used: ATCC 25923 (Staphylococcus aureus), ATCC 35984 (Staphylococcus epidermidis), ATCC 43300 (MRSA, methicillin-resistant Staphylococcus aureus), and MRSE287 methicillin-resistant Staphylococcus epidermidis) MRSE287 was isolated from the prosthetic surface of patients with prosthetic infection after orthopedic joint replacement at the Ninth People's Hospital of Shanghai Jiaotong University School of Medicine. All study participants provided informed consent. After strains were resuscitated, single clonal colonies were collected, cultured in tryptone soy broth (TSB) culture medium, shaken at 37°C with a constant temperature shaker rotating at 120 rpm, and cultured in aerobic conditions for 12-16 h, after which 1 mL of bacterial suspension was collected and centrifuged at 7500 rpm for 5 minutes. The supernatant was discarded and the pelleted bacteria were collected. Culture medium was added to the bacteria and vortexed. The concentration of the bacterial suspension was adjusted to 1×10^6 cfu/mL according to the McFarland turbidimetry method, for later use.

2.6.2. Measurement of bacteriostatic efficacy on the material surface

A pure titanium disc sample was used as a control group; the titanium disc and experimental pure Zn and Zn-Cu alloys wafers were sterilized with ethylene oxide and placed in a 24-well plate well. Bacteriostatic efficiency was measured using a serial dilution plating method. A concentration of 1×10^6 cfu/mL of bacterial suspension was added to the 24-well plate, 1 mL per well, and after 24 h of co-culture, the material sample at the bottom of the well was collected. The sample was gently rinsed three times, with PBS buffer, and the material samples were placed in a sterile glass test tube (1/tube), respectively. TSB medium (0.5 mL) was added dropwise. To separate the bacteria adhering to the surface of the material, an ultrasonic water washing instrument (B3500S-MT, Branson Ultrasonics Co., Shanghai, China) was used to sonicate the tube for 20 min at a frequency of 50 Hz. The sonicated bacterial suspension was diluted through a gradient, and 500 μ L of the suspension was pipetted, plated evenly (on a TSA plate), and then placed in a

37°C incubator for 24 h. The number of colonies on the TSA culture plate was counted, and the bacteriostatic efficiency of each group of Zn–Cu alloy extracts was calculated using pure Ti as the control group.

2.6.3. Antibacterial performance in bacterial suspension

The bacterial suspension at a concentration of 1×10^6 cfu/mL was added to a 24-well plate at 1 mL per well and co-cultured with samples for 24 h. The bacterial suspension was collected and fluorescence-stained using a Live/Dead stain kit (Invitrogen; Eugene, OR). The kit contained two fluorescent dyes, EthD-1 and AM, the former causes dead bacteria to emit red fluorescence, and the latter causes live bacteria to emit green fluorescence. Staining in the bacterial suspension was observed under a laser confocal microscope (Leica TCS, SP2, Germany) at room temperature, after being protected from light for 15 min.

2.6.4. Bacterial morphology on the material surface

The morphological characteristics and changes in bacteria on the surface of the material were observed by scanning electron microscopy after the material samples were co-cultured with the bacteria for 24 h. The material sample was taken out and gently washed three times with PBS buffer. The sample was placed in 2% glutaraldehyde fixative and fixed overnight in a refrigerated environment at 4°C. The sample was rinsed with PBS at 4°C and fixed for 2 h with 1% osmium tetroxide PBS fixative at 4°C. The specimen was washed again with 4°C PBS, dehydrated through a gradient of different concentrations of alcohol (30%, 50%, 70%, 80%, 90%, 95%, 100%, 100%), and then dehydrated twice with isoamyl acetate for 10 min at each time. After critical point drying using a HITACHI HCP-2, BAL-TEC ion sputtering was performed, and the morphology of the bacteria was observed by field emission scanning electron microscopy (FESEM, Hitachi S-4800, CamScan).

2.6.5. Bacterial morphology in bacterial suspension

The sterilized pure Ti and Zn-Cu alloy metal disks were placed in a 12-well plate with three replicate samples in each group, and 2 mL of 1 \times 10⁶ CFU/mL bacterial suspension was added to each well. Bacterial suspensions were collected 24 h after coculture of bacteria with the material samples. After centrifugation and rinsing, bacterial precipitates were collected, fixed, and dehydrated as described above, and stored in absolute ethanol. After critical point drying using a HITACHI HCP-2, BAL-TEC ion sputtering was performed, and the morphology of the bacteria was observed by field emission scanning electron microscopy (FESEM, Hitachi S-4800, CamScan). Additionally, bacterial precipitates were collected, washed with 1% sodium carbonate, centrifuged again, fixed with 2% glutaraldehyde, and observed by transmission electron microscopy (TEM, Hitachi-7600 machine, Tokyo, Japan).

2.6.6. Expression of bacteria-related genes (real-time PCR)

Based on the results of the above-mentioned studies on the anti-infection properties of the Zn–Cu alloys, we selected the Zn–2Cu alloy for further studies on the anti-infection mechanism. The pathogenic strain ATCC 43300 (MRSA), which is common in osteomyelitis infections, was selected as the pathogenic bacteria, and real-time PCR was used to determine the expression of MRSA bacteria-related genes in the Zn–2Cu alloy extract, including icaA, icaB, icaC, icaD, icaR, SigB, and Spa, associated with bacterial biofilms; SarA, lytM, lytR, ArlR, and ArlS, associated with bacterial autolysis; MurC, MurE, and saeR, associated with bacterial wall synthesis; clfA and atlE, associated with bacterial adhesion; PBP2a, MecA, FemA, FemB, and FemX, associated with bacterial drug resistance; and empbp and ssaA, associated with bacterial virulence. Bacterial suspension at a concentration of 10⁶ cfu/mL was added to a 24-well plate containing a Zn–2Cu alloy disc and a Ti disc (for

the control group) for 24 h, after which the bacterial suspension was centrifuged to collect the bacterial pellet, and RNAprotect Bacteria Reagent solution was added to dissolve the RNA to ensure its integrity. After centrifugation, the bacteria were lysed using TE buffer containing 100 $\mu g/mL$ of lysostaphin (Sigma) and incubated at 37°C for 10 minutes. Gene expression was assessed as described in 2.6.3. The details of the primers are shown in Table S2.

2.7. Animal experiments

2.7.1. Surgical procedure

All animal operations and experiments were approved by the Animal Ethics Committee of the Ninth People's Hospital affiliated to Shanghai Jiao Tong University. Thirty-six male Sprague Dawley rats were used. A rat femur intramedullary nail infection prevention model was established, and surgery was performed under aseptic conditions. Rats were anesthetized by intraperitoneal ketamine injection (10 mg/kg, Shanghai Ziyuan Pharmaceutical Co. Ltd, Shanghai, China) and 2% xylazine (5 mg/kg, Bayer AG, Leverkusen, North Rhine-Westphalia, Germany). A subcutaneous injection of 0.3 mg/kg buprenorphine (Temgesic, Reckitt & Cloman, Hull, UK) was given for postoperative analgesia. The right hind limb of the rat was shaved and the knee joint was fixed at the maximum flexion position. After palpating the patella, a 15-mm longitudinal incision was made along the lateral side of the patella, the layers of tissues were separated individually, the knee joint was dislocated, the femoral condyle was fully exposed, and an electric drill was used to drill along the direction of the medullary cavity at the center of the femoral condyle. After rinsing the bones with normal saline to remove debris, sterile forceps were used to implant a small cylindrical material immersed in MRSA bacteria suspension at a concentration of 1×10^7 cfu/mL for 10 minutes, into the bone canal; finally, bone wax was used to seal the bone, and the wound was sutured. The rats were euthanized at 3 and 6 weeks after surgery. The surgical groups were as follows: (1) sham operation group (n = 12): healthy rats were closed immediately after incision; (2) Ti control group (n = 12): a pure Ti cylinder immersed in bacterial suspension was implanted into the medullary cavity; (3) Zn-2Cu alloy group (n = 12): a Zn-2Cu alloy cylinder immersed in bacterial suspension was implanted into the medullary cavity.

2.7.2. X-ray observation

Rat femurs were imaged under operating conditions using X-ray machines (52 kV and 3.2 mAs, Digital Diagnost, Philips, Amsterdam, Netherlands) at 0, 3, and 6 weeks and the implants were assessed.

2.7.3. In vivo biosafety

The general characteristics of the experimental animals, including body temperature, body weight, and wound healing, were recorded daily after surgery. Six weeks after the model establishment operation, blood was randomly collected from the hearts of the experimental animals in the three groups (Blank, Ti, and Zn–2Cu alloy). Subsequently, routine blood work, serum metal ion concentration, and blood biochemical tests were performed, and the indices of healthy blood samples were used as controls. At 6 weeks after operation, the heart, liver, spleen, lung, kidney, and prostate of the Zn–2Cu alloy group were collected. The Zn²⁺ and Cu²⁺ contents in the organs of the experimental group were determined by ICP-mass spectrometry (NexION 300 ICP-MS, PerkinElmer, USA). Samples were fixed, embedded, sectioned, and stained with HE to observe any pathological changes in each organ. Healthy rats were used as controls.

2.7.4. Histology

Rat femur specimens with the nails removed were fixed in 4% paraformaldehyde, decalcified in 10% EDTA for approximately 6

weeks, dehydrated through an ethanol gradient, and embedded in paraffin. Next, HE, Gram, Giemsa, Masson, Van Gieson, and Trap staining were performed. The specimens were examined and photographed using a high-quality microscope (Olympus CKX41, Olympus Co. Ltd., Tokyo, Japan) and an automatic digital slide scanner (Pannoramic MIDI, 3D HISTECH, Budapest, Hungary).

2.7.5. Culture of bacteria from implants and surrounding tissue

At week 6 after surgery, the implants and surrounding bone tissue were collected. After isolation by ultrasonication, bacteria were cultured, plated, and counted to assess the *in vivo* bacteriostatic efficiency of the Zn–2Cu alloy implants. To check whether the ultrasonically detached bacteria were MRSA pathogens, their resistance to methicillin was confirmed by PCR detection of mecA gene expression. [10,36].

2.8. Data analysis

Data analysis was performed using SPSS 18.0 statistical software (SPSS Inc. Chicago, USA). Quantitative data are expressed as mean \pm standard deviation (SD). Data were analyzed using the *t*-test for independent samples, one-way analysis of variance (ANOVA), Tukey's and Bonferroni multiple comparison test. Differences were considered statistically significant at p < 0.05 or p < 0.01.

3. Results

3.1. Microstructure and mechanical properties

Fig. 1 shows the microstructure of the experimental pure Zn and Zn-Cu alloys. Tiny precipitates were visible in Zn-0.5Cu and Zn-1Cu alloys, and the intermetallic phase became much larger in the Zn-2Cu alloy. The alloy grain grew after adding Cu but the grain size then decreased with the Cu contents. The grain size increased in Zn-0.5Cu alloy while both fine and coarse grains can be observed at Zn-2Cu alloy. The refined grains are usually surrounding the second phases. XRD detected no peaks of second phases at Cu contents < 1 wt%, due to the relatively high solubility of Cu in Zn (2.75 wt% at 425°C). The Zn-2Cu alloy comprised a CuZn_5 and Zn matrix. The mechanical properties of the pure Zn and Zn-Cu alloys are shown in Fig. 1c-e. As the Cu contents increased, the ultimate tensile strength and yield strength increased remarkably. A similar trend could be seen in compressive strength and microhardness. In addition, the stress-strain curves of pure Zn and Zn-Cu alloys for tensile and compressive tests were showed in Figure S2. Among the experimental Zn-Cu alloys, the optimum composition was the Zn-2Cu alloy, showing the highest strength (YS 226 MPa, UTS 270 MPa). Moreover, adding Cu had no detrimental effect on the ductility of Zn, and the elongation of the Zn-2Cu alloy was still around 41%.

3.2. Degradation behavior

The surface morphology of the specimens before and after removal of the degradation products are presented in Fig. 2a. All the samples had similar corrosion morphology before cleaning. After removal of the degradation products, the Zn-Cu alloys displayed a rougher surface morphology than that of pure Zn. In Zn-2Cu alloy, the intermetallic phase remained intact whereas the surrounding Zn was corroded severely, indicating a typical galvanic corrosion mode. The corrosion rates of the Zn-Cu alloys increased significantly with Cu contents, and they were doubled in the Zn-2Cu alloy (Fig. 2b). EDS showed that the primary chemical composition of the degradation products was composed of Zn, C, O, and P (Fig. 2c).

3.3. Cytocompatibility and osteogenic differentiation

Fig. 3a shows the viability of MC3T3-K cells after 24, 48, and 72 h of co-culture with pure Zn and Zn-Cu alloy extracts, and the ion concentrations in extracts are listed in Table S3. One-fold and two-fold diluted material extracts were used for cytocompatibility testing based on the industry consensus [37]. In the one-fold diluted extract group, we found that the viability of MC3T3-K cells in the pure Zn extract was significantly reduced at all three time points compared to the control group, and there was no significant improvement in the Zn-0.5Cu alloy group. In contrast, a significantly better performance was found on the Zn-1Cu and Zn-2Cu alloy extracts, which showed a similar OD value to that of the control group. In the co-culture with two-fold diluted extracts, the viability of MC3T3-K cells co-cultured with Zn-0.5Cu, Zn-1Cu, and Zn-2Cu alloy extracts was significantly improved compared to that in the pure Zn and the control groups. According to ISO 19003-5 [38], the results suggested that pure Zn was cytotoxic to MC3T3-K cells, whereas adding Cu significantly improved the cytocompatibility of pure Zn. The Zn-2Cu alloy had the best cytocompatibility among all the experimental materials. Fig. 3b further illustrates the effect of one-fold diluted material extracts on the morphology of MC3T3-K cells using Live/Dead cell staining and cytoskeletal staining. Pure Zn and Zn-0.5Cu groups had sparse, lowintensity green fluorescence, whereas the fluorescence intensity of the Zn-1Cu group was greatly elevated, and the fluorescence intensity of the Zn–2Cu group was close to that of the control group. Cytoskeletal staining further revealed that the cells in the pure Zn and Zn-0.5Cu alloy groups exhibited marked shrinkage and poor spreading, the cells in the Zn-2Cu alloy group showed a substantial degree of spreading, and the red tensile filaments composed of actin were fully spread. These results confirmed the good cytocompatibility of Zn-Cu alloys, among which Zn-2Cu alloy being the most cytocompatible.

The effects of the diluted material extracts on the osteogenic differentiation of MC3T3-K cells were studied by testing ALP activity both qualitatively and quantitatively (Fig. 3c, d). After one-fold dilution, the osteogenic differentiation in the pure Zn and Zn–0.5Cu alloy groups was still inhibited compared to that in the control group. Nevertheless, Zn–1Cu and Zn–2Cu alloy groups displayed comparable osteogenic differentiation abilities to that of the control group. After two-fold dilution, there was no significant difference among the pure Zn, Zn-0.5Cu alloy, and the control groups in osteogenic differentiation, whereas the Zn–1Cu and Zn–2Cu alloy groups were even better than the control group. The expression of osteogenic differentiation related genes was further evaluated and are presented in Fig. 3e. The expression of ALP, COL 1, OCN, and Runx-2 genes, which are associated with osteogenic differentiation demonstrated the same tendency as the ALP results.

3.4. In vitro anti-infection performance

3.4.1. Bacteriostatic efficacy on the sample surface

The bacteriostatic efficacy of the pure Zn, Zn–1Cu, and Zn–2Cu alloy was assessed using the plating gradient dilution method (Fig. 4a, b). The pure Zn group exhibited a significantly higher antibacterial activity compared to the control group after 24 h of bacterial co-culture. In contrast, the bacteriostatic efficacy of Zn–Cu alloys on all four bacterial strains was significantly higher than that of the pure Ti and pure Zn groups. A large number of clonal bacterial colonies were observed in the pure Ti group, whereas no bacterial colonies were visible in the Zn–2Cu alloy group. Two drugresistant bacterial strains (ATCC43300 and MRSE287) were selected to observe their adhesion on the specimen surface (Fig. 4c). A large amount of bacterial growth, which resulted in clusters and multilayered accumulations with composite morphology, was visualized

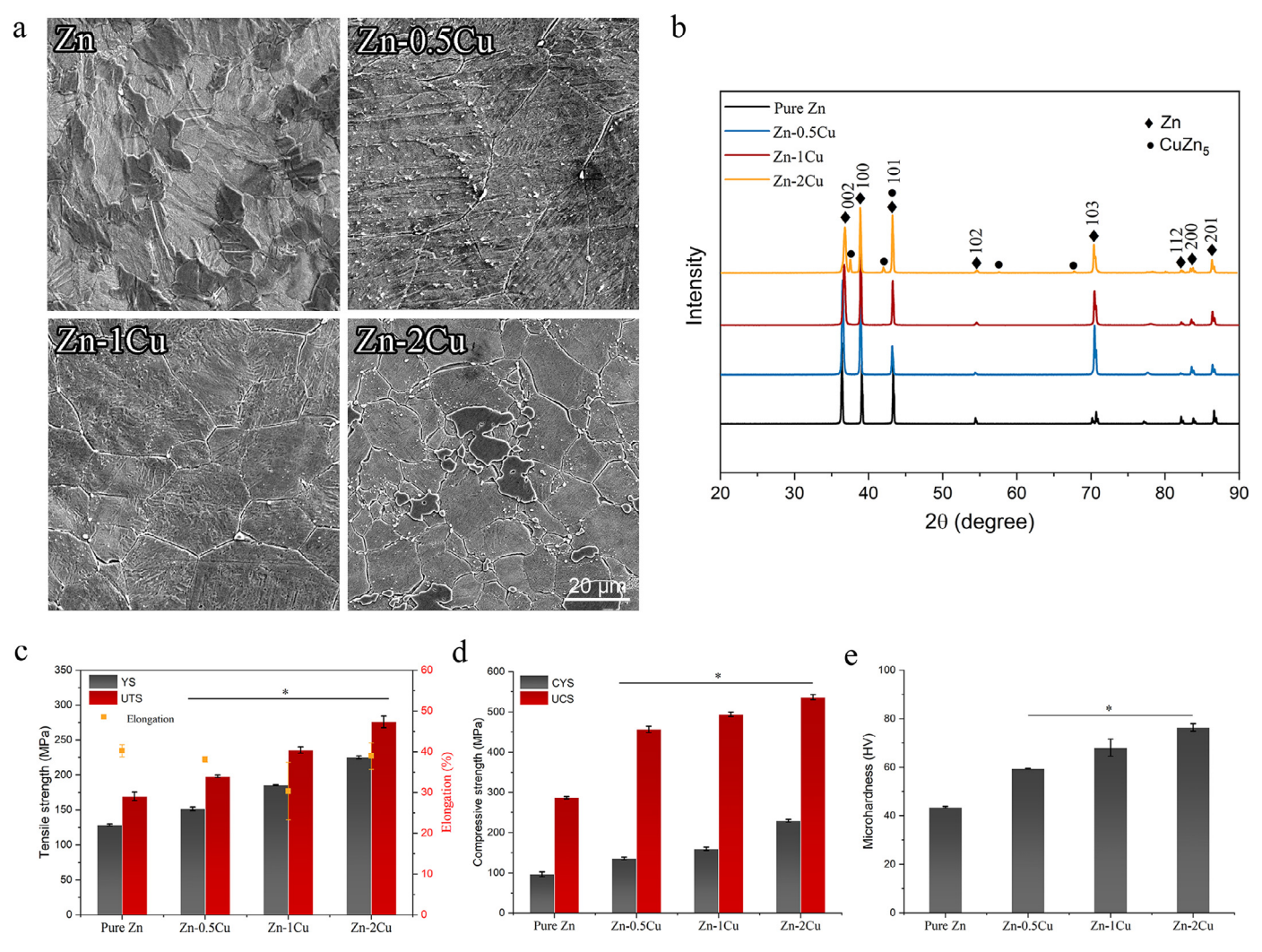


Fig. 1. (a) SEM images of pure Zn and Zn-Cu alloys, (b) XRD, (c) tensile test, (d) compressive test, and (e) microhardness of pure Zn and Zn-Cu alloys.

on the surface of pure Ti. Only a few bacterial colonies formed on the pure Zn surface. In contrast, limited amounts of bacteria adhered to the surface of Zn–1Cu and Zn–2Cu alloys. More importantly, the bacterial cells on the surface of the Zn-Cu alloys exhibited morphologies of shrinkage, distortion, and even dissolution and rupture.

3.4.2. Bacteriostatic efficacy in bacterial suspension

The bacteriostatic activity on the bacterial suspension after coculture with the experimental samples was observed using laser confocal microscopy (Fig. 5). The pure Ti group (control group) showed high intensity of green fluorescence, indicating the formation of a bacterial biofilm. In the pure Zn group, the fluorescence intensity was significantly reduced. In contrast, only a small number of weak fluorescent spots were observed in the Zn-Cu alloy groups, and almost no live bacteria were detected in the Zn-2Cu group.

The morphology and structure of bacteria in the suspension was further observed by SEM and TEM (Fig. 6a). The bacteria showed a healthy morphology and normal binary fission on the surface of pure Ti and pure Zn groups. In contrast, the bacterial morphologies were abnormal after co-culture with the Zn-1Cu and Zn-2Cu alloy extracts. The TEM images revealed swelling and dissolution of the bacterial wall and membrane, and cells in the dividing phase were disrupted substantially.

MRSA (ATCC43300) was chosen to study the effect of Zn-2Cu alloy on the expression of bacterial behavior-related genes (Fig. 6b), with pure Ti as the control. In general, the expression levels of biofilm-related genes (icaA, icaB, icaC, icaD, and SigB), autolysis-related genes (lytM, lytR, ArlR, and ArlS genes), and adhesion-related genes (atlE gene), were downregulated significantly compared to those with pure Ti. Similar trends were also found in cell wall synthesis-related genes (MurC and MurE genes), resistance-related genes (PBP2a, MecA, FemA, FemB, and FemX genes), and bacterial virulence-related genes (empbp and ssaA genes).

3.5. In vivo anti-infective performance

3.5.1. X-ray results and anti-infective performance

Zn-2Cu alloy and pure Ti rods immersed in MRSA bacterial suspension were implanted into the rat femur, with a sham operation group as the control. The body temperature of the pure Ti group was remarkably elevated, whereas the body weight was reduced during the entire implantation period in contrast to the Zn-2Cu and sham operation groups (Fig. 7a). X-ray imaging results are shown in Fig. 7b. Compared to the sham operation group, the pure Ti group showed signs of osteomyelitis, presenting as obvious cortical bone destruction and periosteal reaction. The osteomyelitis and periosteal reaction was much milder in the Zn-2Cu alloy group, with scores significantly lower than those of the

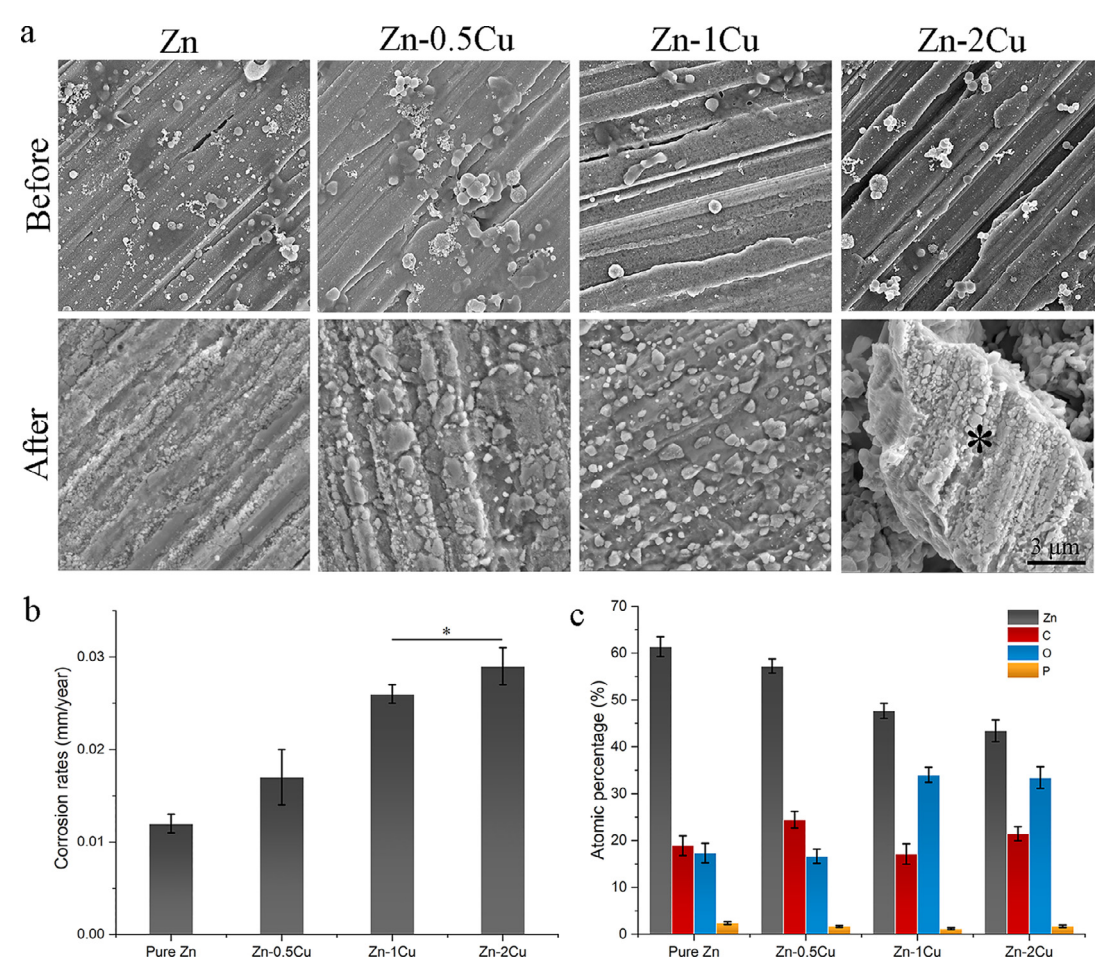


Fig. 2. (a) Corrosion morphology before and after removal of corrosion products following 30 days' immersion in SBF solution, the intermetallic phase is marked by *, (b) corrosion rates and (c) chemical composition of corrosion products.

pure Ti group, suggesting an anti-infection property of the Zn-2Cu alloy (Fig. 7c). The implants were further harvested to evaluate their bactericidal performance both qualitatively and quantitatively (Fig. 7d, e). Large amounts of bacteria were isolated from both the pure Ti implant and surrounding bone tissue, whereas significantly lesser bacteria were found in the Zn-2Cu group. The Zn-2Cu alloy showed significantly higher antibacterial activity than that of pure Ti at both time points (p < 0.01).

3.6.2. Histological assessment

HE staining of the femoral medullary cavity of each group is presented in Fig. 8. Notable intramedullary abscess formation was observed in the pure Ti group. A large amount of inflammatory cell infiltration was found in the infected lesions. In contrast, MRSA-induced infection in the Zn–2Cu alloy group was generally controlled, but a mild inflammatory reaction was still visible. This may be related to the stimulation of surrounding tissues by the degradation products of the Zn–2Cu alloy. Additionally, Gram staining showed a large amount of bacterial counterstaining (blue) in the medullary cavity of the pure Ti group, but no bacterial staining was found in the control and Zn–2Cu alloy groups. Giemsa staining revealed similar results; remarkable bacterial aggregates (red arrows) could be seen in the medullary cavity of the pure Ti group, but few bacteria were found in the Zn–2Cu alloy group.

To evaluate the biosafety of Zn-2Cu implants, Masson and Van Gieson staining of the femoral medullary cavity were performed (Fig. 9). There was more immature new bone formation (usually

sequestrum) in the pure Ti group, whereas the Zn–2Cu group had a better bone mass than the blank control group. TRAP staining revealed more osteoclastic bone resorption in the pure Ti groups, whereas little indication of bone resorption was observed in the blank control and Zn–2Cu alloy group.

3.6.2. Systemic toxicity

The results of blood indices are shown in Table S4-6. The infection-related indices, such as white blood cell count, neutrophil ratio, and absolute neutrophil count were elevated in the pure Ti group, whereas these indices were within the normal range in the Zn-2Cu alloy group. The concentrations of the serum metal ions including Ca, Mg, Zn, and Cu showed no statistically significant difference among all the groups. Additionally, the LDH1 index of blood biochemical tests was significantly elevated in the pure Ti group, indicating potential myocardial injury. The Zn²⁺ and Cu²⁺ ion concentration and organ pathology sections in the Zn-2Cu alloy group are as shown in Fig. 10. Additionally, no abnormality was observed in the pathological sections and ion concentrations in important organs of the of Zn-2Cu group compared to the healthy group. These results indicate satisfactory *in vivo* biosafety of the Zn-2Cu alloy.

4. Discussion

Biodegradable metals provide a major advantage over the traditional Co-Cr and Ti-based materials in the context of antibacterial implants as the disappearance of these implants after bone heal-

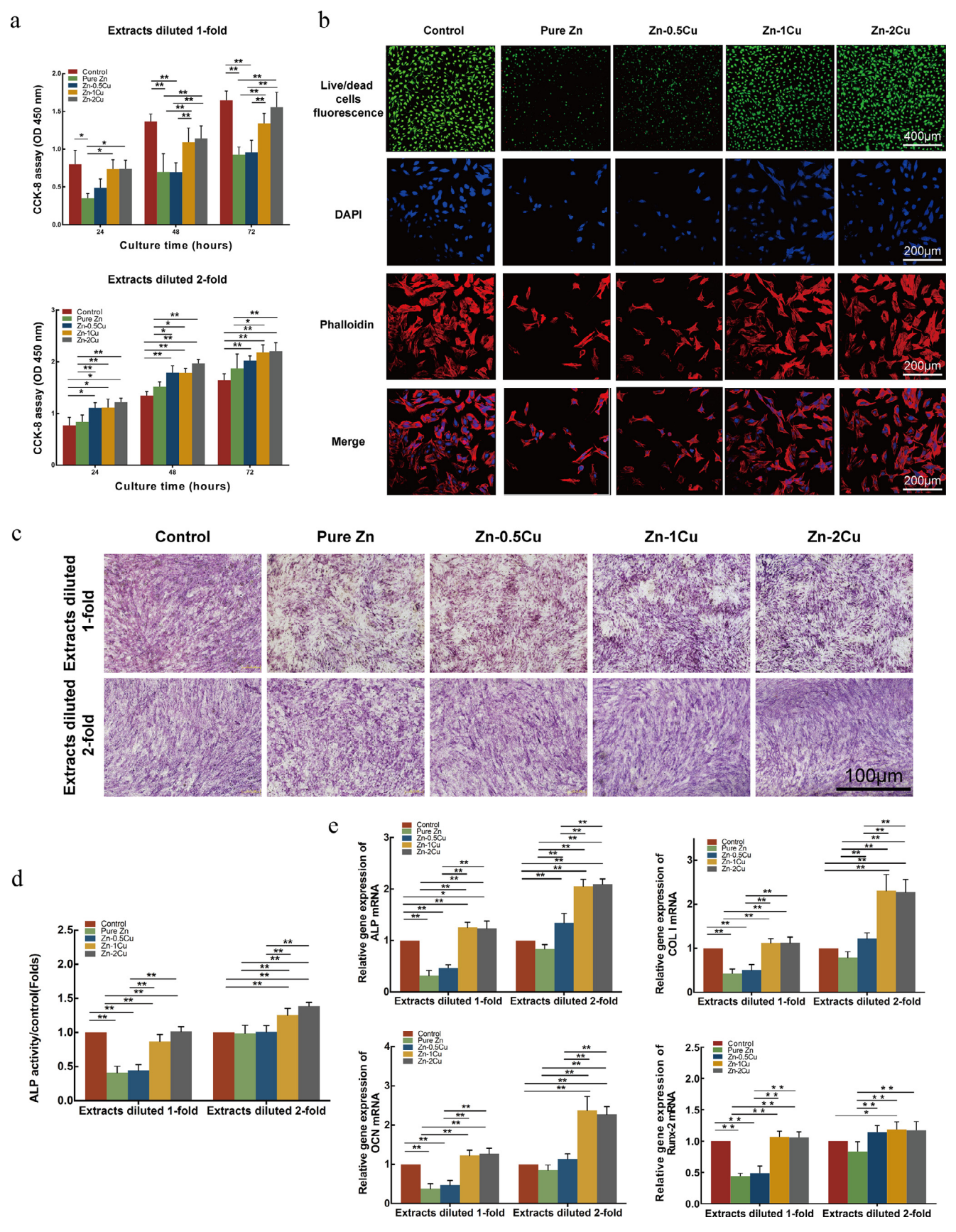


Fig. 3. (a) Proliferation of MC3T3-K cells cultured with pure Zn and Zn-Cu alloy extracts (1-fold and 2-fold dilutions) for the indicated times (* p < 0.05; ** p < 0.01). (b) Live/dead cell staining and cytoskeletal staining for MC3T3-K cells cultured with pure Zn and Zn-Cu alloy extracts. For Live/Dead cell staining, live cells were stained with green fluorescence, and dead cells were stained with red fluorescence. Representative images of cells stained with TRITC-phalloidin for actin filaments (red) and DAPI for cell nuclei (blue). (c) ALP staining, (d) ALP activity, and (e) relative expression of osteogenic differentiation marker genes in MC3T3-K cells cultured for 10 days in osteogenic medium with pure Zn and Zn-Cu alloy extracts. Data represent mean \pm standard deviation. (*p < 0.05; ** p < 0.01)

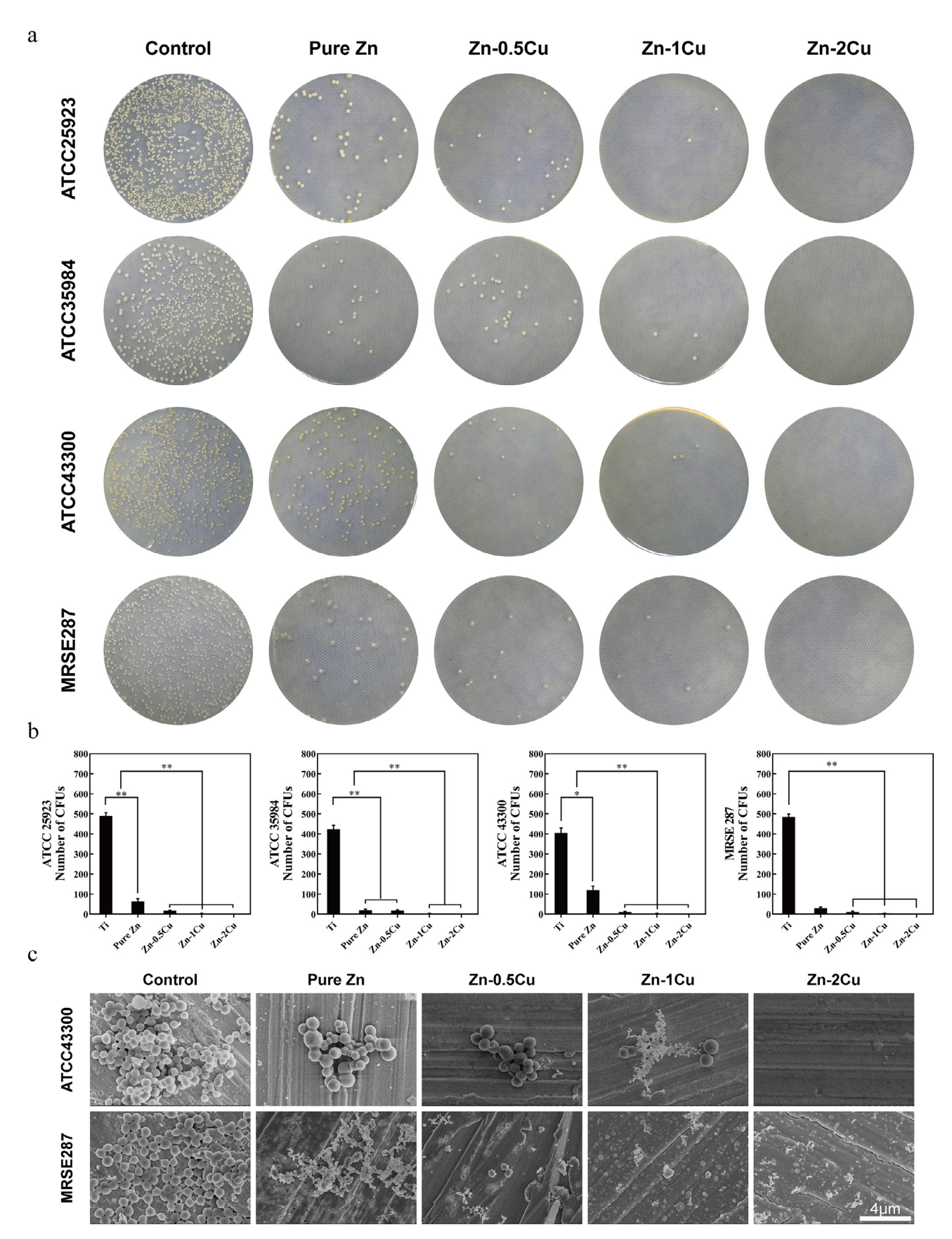


Fig. 4. (a) Representative images of bacteria grown on the surface of samples after 24 h of culture, with pure Ti as control. (b) Colony counts of ATCC25932, ATCC35984, ATCC43300, and MRSE287 bacteria on the sample surfaces after 24 h of culture. (c) Bacterial morphologies of the ATCC43300 and MRSE287 strains on sample surfaces after 24 h of culture, with pure Ti as the control.

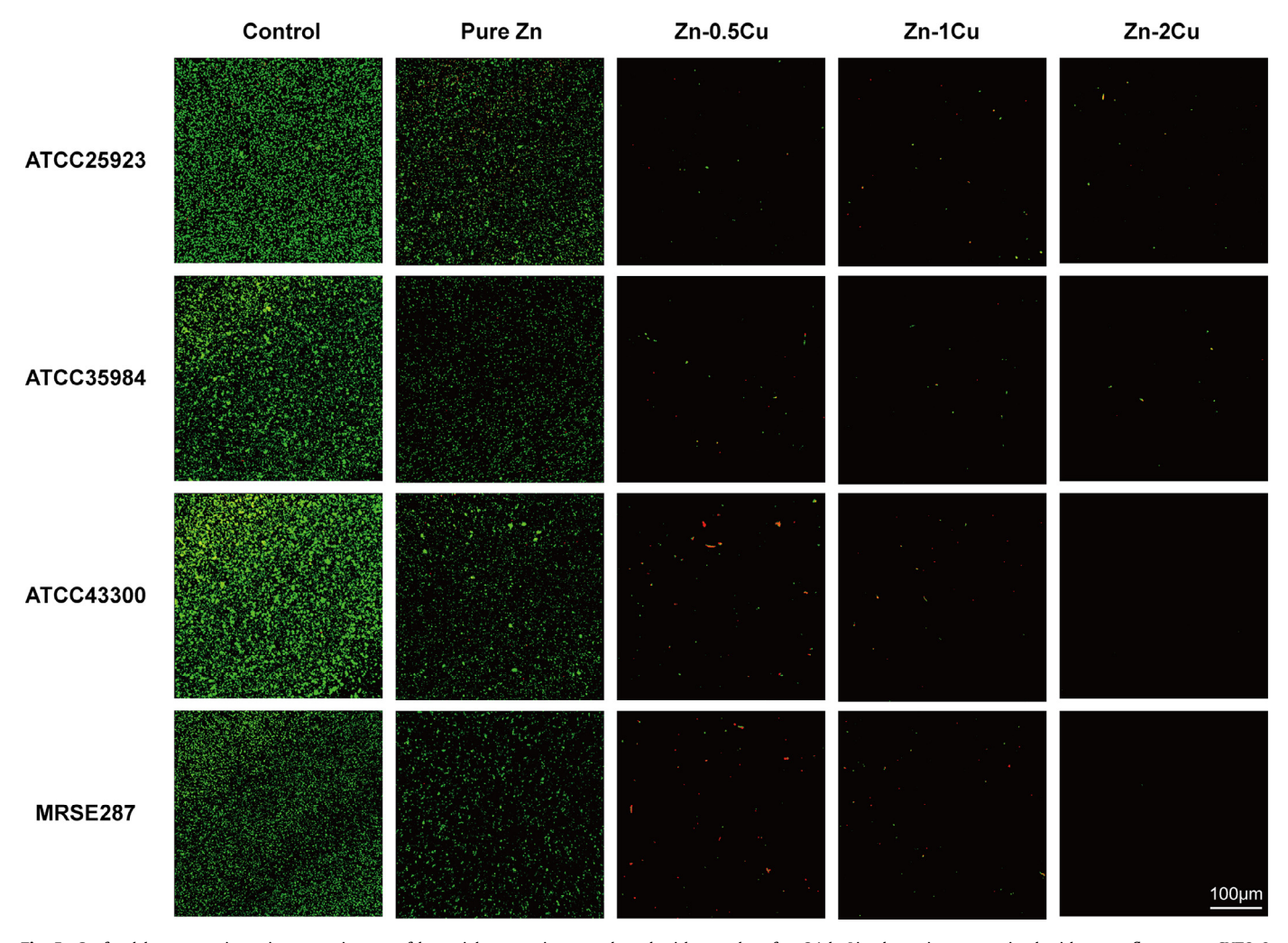


Fig. 5. Confocal laser scanning microscopy images of bacterial suspension co-cultured with samples after 24 h. Live bacteria were stained with green fluorescent SYTO 9, and dead bacteria were stained with red fluorescent propidium iodide, with pure Ti as control.

ing will deprive the bacteria of their necessary habitat. Biodegradable Mg-based materials have been considered a promising choice because of the wide research on them in treating fractures or other orthopedic injuries in animal and clinical studies [39–67]. Our previous study demonstrated a systematic in vitro and in vivo characterization of Mg-Cu alloys in terms of antibacterial performance and mechanism [68], and revealed that Mg-Cu alloys exerted antibacterial activity by inhibiting bacterial adhesion and biofilm formation. However, their future clinical application could be strictly limited due to their relatively fast corrosion rate, low mechanical strength, local accumulation of released hydrogen, and pH elevation. Recently, our team and co-workers have extensively researched Zn-based materials as alternatives for orthopedic implants [22,69-73]. The results showed that Zn-based implants demonstrated a prospective performance regarding mechanical property, degradation behavior, and osteogenic capability. We also found that Zn alone displayed a certain inhibitory effect on bacteria. Zn-Cu alloys with desirable mechanical performance (YS 250 \pm 10 MPa, UTS 270 \pm 10 MPa, and elongation 51 \pm 2 %) have been recently developed for orthopedic applications [23,35]. Moreover, Wen and colleagues developed Zn-Cu alloys and Zn-1Cu-0.1Ti alloys and examined the antibacterial activity by inhibition zone diameter method of Zn-Cu alloys against S. aureus in vitro [74,75]. Another team developed Cu 17%Ni 10%Zn-coated 316L stainless steel and found preliminarily antibacterial properties in vitro [76]. The addition of Cu resulted in significant increase in strength while the ductility of Zn was maintained. This unique advantage of Zn-Cu alloy can be attributed to (1) the CuZn₅ has the same crystal structure as Zn, i.e. dense-hexagonal crystal, which leads to compatible deformation; (2) the gradient fine-grain and coarse grain architecture enhance the strength-plasticity synergy [77]. However, limited information is available regarding the capability of Zn-Cu alloys against different bacterial species and their underlying antibacterial mechanism. Therefore, we assessed the antibacterial performance of Zn-Cu alloys and examined the underlying mechanism by combining in vitro and in vivo experiments. The present study provides compelling evidence from findings that Zn-Cu alloys had high anti-bacterial efficacy against both coagulase-positive staphylococci (MRSA and S. aureus) and coagulase-negative staphylococci (MRSE and S. epidermidis) by preventing pathogen adhesion and biofilm development. Next, we evaluated the in vivo anti-infection efficacy of the Zn-2Cu alloy using a rat femoral intramedullary nail MRSA infection model. Implants made of the Zn-2Cu alloy exerted effective bacterial-killing capability and inhibited the inflammatory and toxic side-effects induced by MRSA bacteria in the rat femur.

The process from bacterial adhesion to effective infection of an internal implant is complicated and involves bacterial wall synthesis, adhesion, colonization, biofilm formation, autolysis, and secretion of virulence factors. The proposed anti-microbial mechanism of Zn-2Cu alloy against MRSA is shown in Fig. 11. The results of bacterial culture plating, CLSM, and SEM observations re-

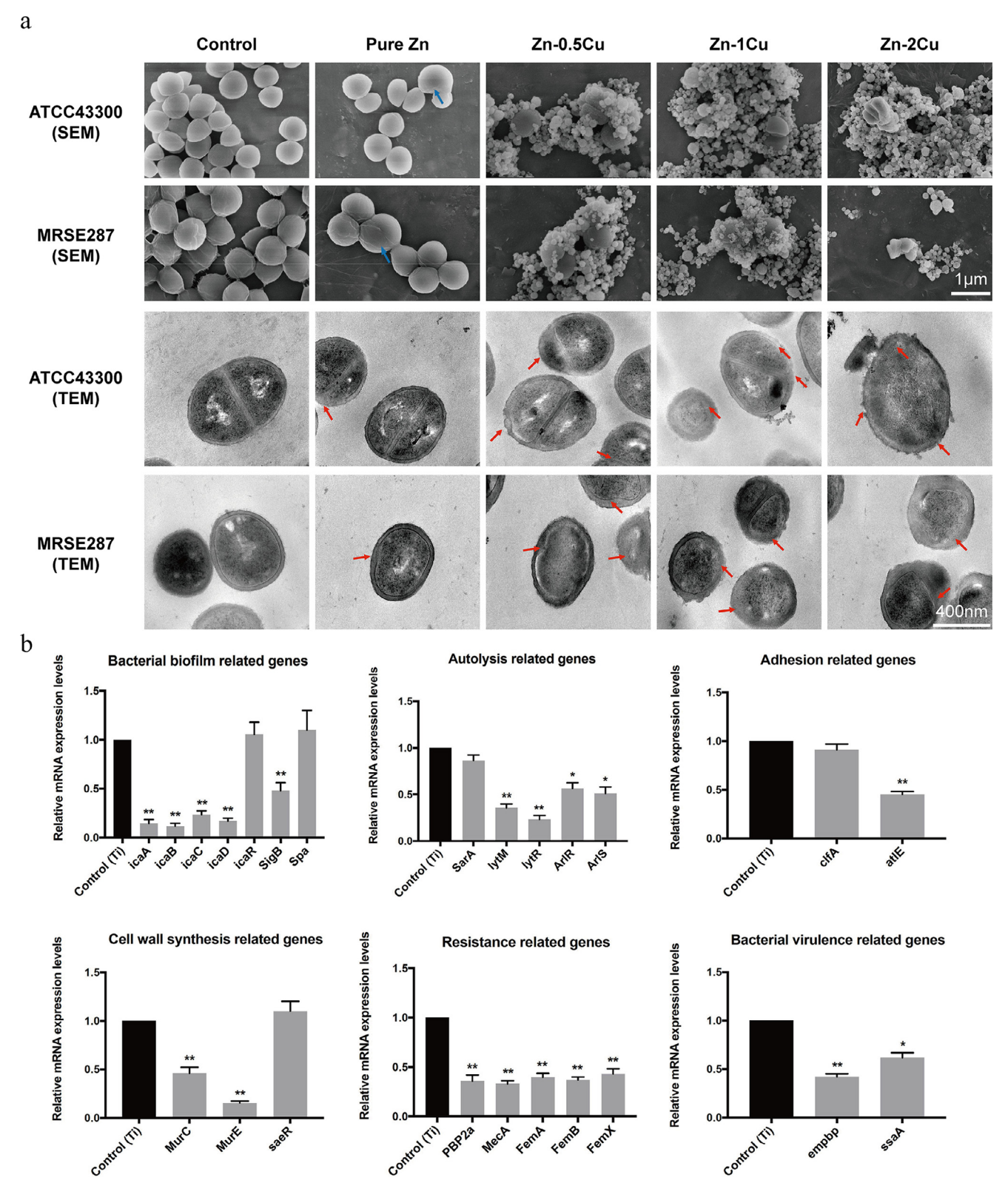


Fig. 6. Bacteria morphologies of ATCC43300 and MRSE287 strains visualized by (a) SEM and (b) TEM in the suspension after 24 h of culture. Red arrows indicate the abnormal morphology of bacteria. (b) Real-time quantitative reverse transcription PCR analysis of genes associated with biofilm formation (icaA, icaB, icaC, icaD, icaR, SigB, Spa), autolysis (SarA, lytM, lytR, ArlR, ArlS), adhesion (clfA, atlE), cell wall synthesis (MurC, MurE, saeR), resistance (PBP2a, MecA, FemA, FemB, FemX), and bacterial virulence (empbp, ssaA). The mRNA levels are the relative mRNA levels compared to those in the Ti control group. Mean \pm SD, * p < 0.05; ** p < 0.01. (For interpretation of the references to color in this figure legend, the reader is referred to the web version of this article.)

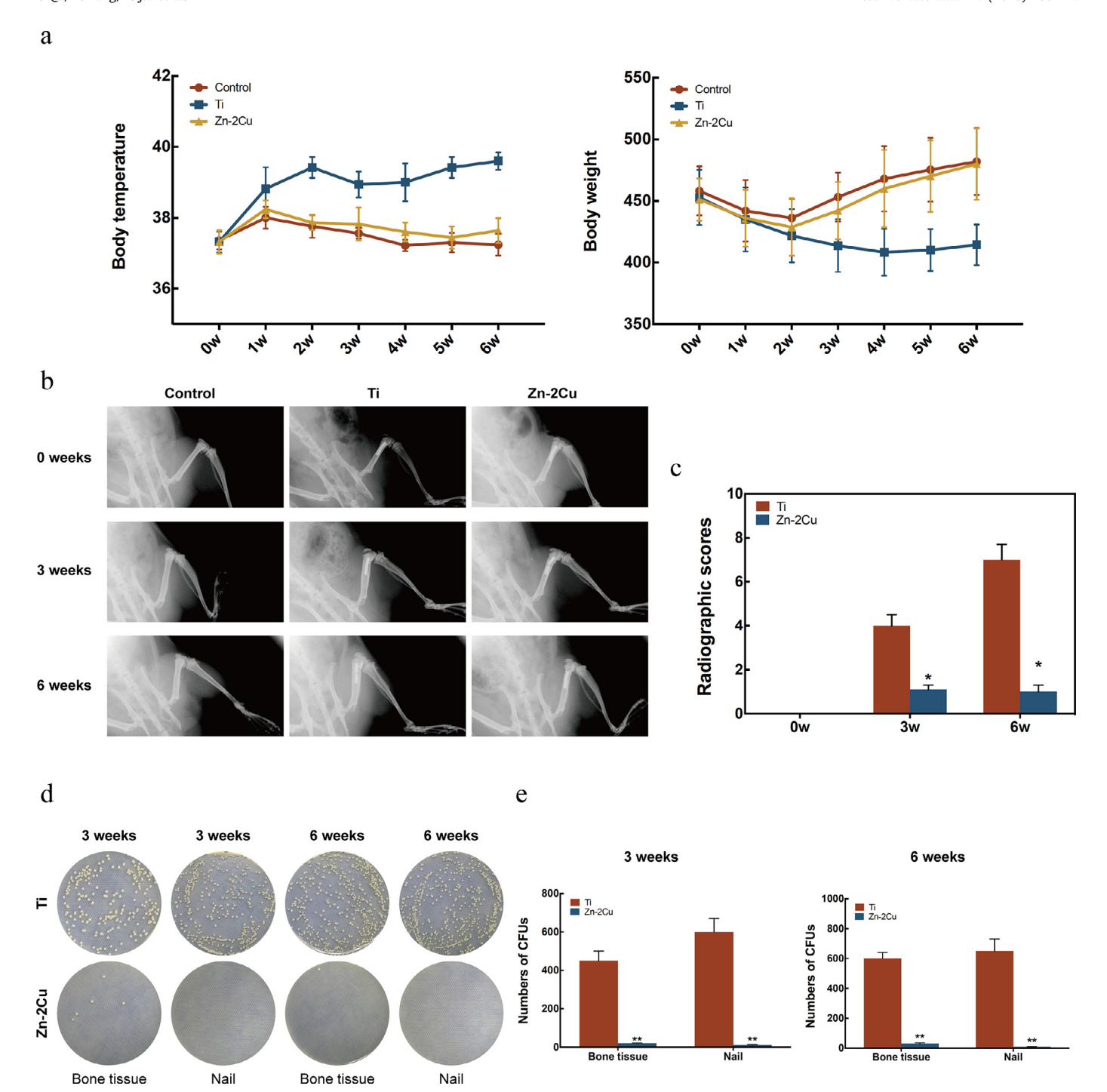


Fig. 7. (a) Body temperature and body weight of animals at selected time points after implantation, (b) X-rays of rat femurs taken at 0, 3, and 6 weeks after implantation, (c) Radiographic scores, (d) representative images of bacterial cultures obtained using the sonication method at 3 and 6 weeks, (e) number of bacterial colonies in the peri-implant bone tissues and on the implanted nails. Mean \pm SD, * p < 0.05; ** p < 0.01.

vealed that the Zn–2Cu alloys inhibited the adhesion and growth of two coagulase-positive staphylococci (MRSA and *S. aureus*) and two coagulase-negative staphylococci (MRSE and *S. epidermidis*) significantly. TEM revealed the abnormal morphology of bacteria co-cultured with Zn-2Cu alloy, showing edema, dissolution, and rupture of the bacterial wall and membrane. It is worth noting that this abnormal morphology of bacteria co-cultured cannot be directly attributed to genetic changes. This phenomenon may be due to corrosion products, certain physical and chemical interactions between oxides or ions, and impaired protein synthesis.

We further investigated the bacteriostatic efficacy of Zn-2Cu alloys at the genetic level. The expression of genes associated with bacterial wall synthesis including MurC and MurE were significantly inhibited as per the PCR results [78]. The atlE gene encodes cell wall autolysin (AtlE) [79,80], which mediates direct adhesion through hydrophobic changes, and indirect adhesion is mediated by polysaccharide intercellular adhesin during the early infection stages. Meanwhile, the clfA gene encodes clumping factor A, a protein adhesin that also regulates adhesion of bacteria at early infection stages [81]. The Zn-2Cu alloy group significantly downregulated the expression of the atlE and clfA genes,

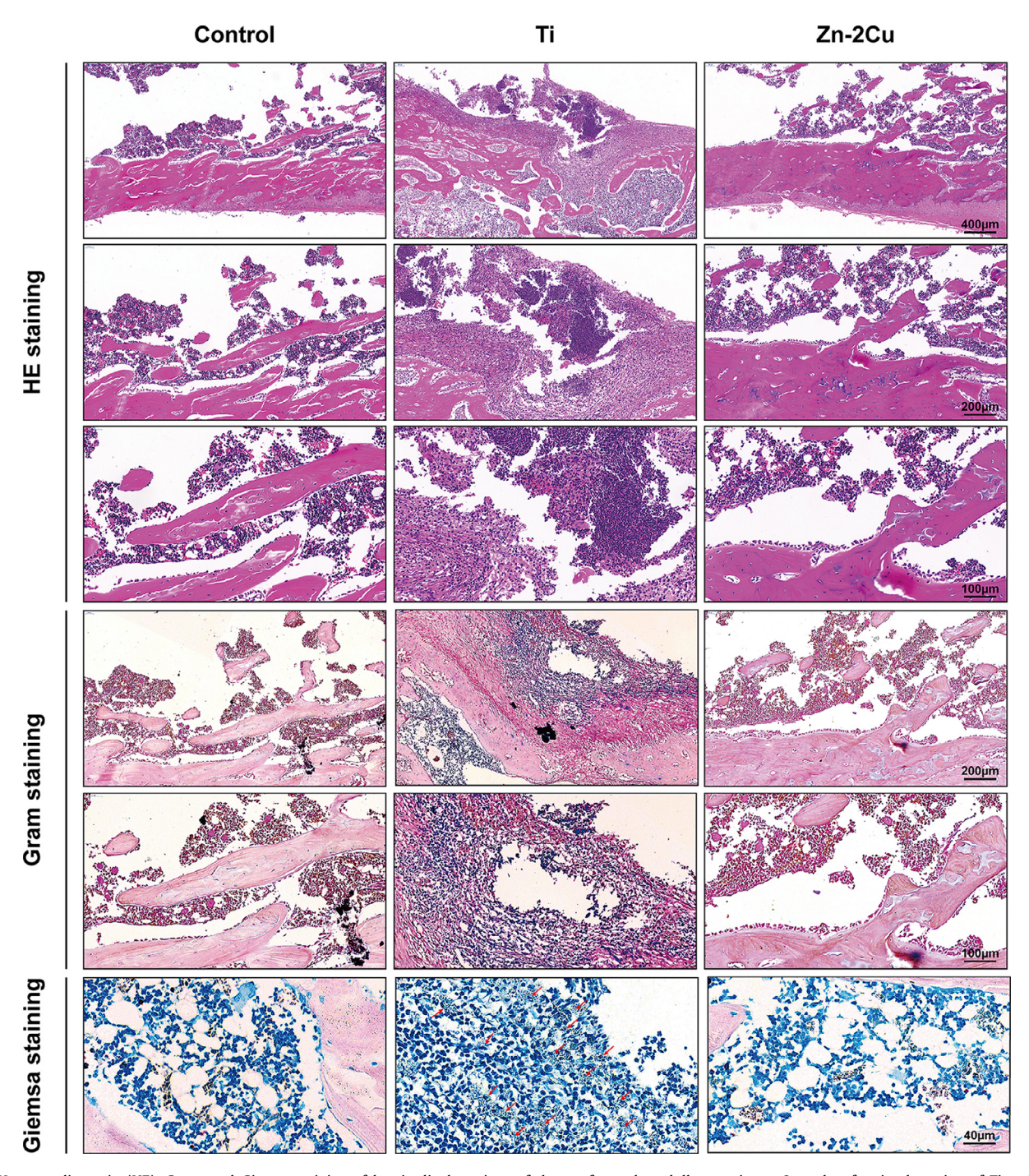


Fig. 8. Hematoxylin-eosin (HE), Gram, and Giemsa staining of longitudinal sections of the rat femoral medullary cavity at 6 weeks after implantation of Ti and Zn–2Cu intramedullary nails. Red arrows show bacterial aggregates. (For interpretation of the references to color in this figure legend, the reader is referred to the web version of this article.)

suggesting effective inhibition of the early adhesion of MRSA on the implant surface. Biofilm formation is critical for effective infection as a biofilm can resist both the immune system and antibiotics. Hence, prevention of biofilm formation is important in preventing and treating infections. The results of CLSM showed that the biofilm was disrupted significantly in the Zn–1Cu and Zn–2Cu alloy groups. The thickening stage of biofilm formation is primarily mediated by the polysaccharide intercellular adhesin (PIA)-dependent and PIA-independent mechanisms. The primary genes encoding PIA are icaA, icaD, icaB, and icaC, which are negatively regulated by the icaR gene [82]. The gene sigB also plays an important role in bacterial biofilm formation, by regulating biofilms

via the ica operon [83–85]. Abnormal biofilm formation is primarily mediated through the function of extracellular matrix proteins such as protein A (Spa) and biofilm-associated protein (Bap) [86]. We found that the Zn–2Cu alloy significantly downregulated the expression of icaA, icaB, icaC, icaD, icaR, and SigB, but did not affect Spa, suggesting that it may disrupt bacterial biofilm formation through the PIA-dependent pathway. Bacterial autolysis is a self-destructive phenomenon that microorganisms undergo in environments not conducive to their own growth. It is manifested as bacterial lysis and release of extracellular DNA, which is important in regulating the early adhesion of bacteria to the surface of implants and to other bacteria, and plays an important role in sta-

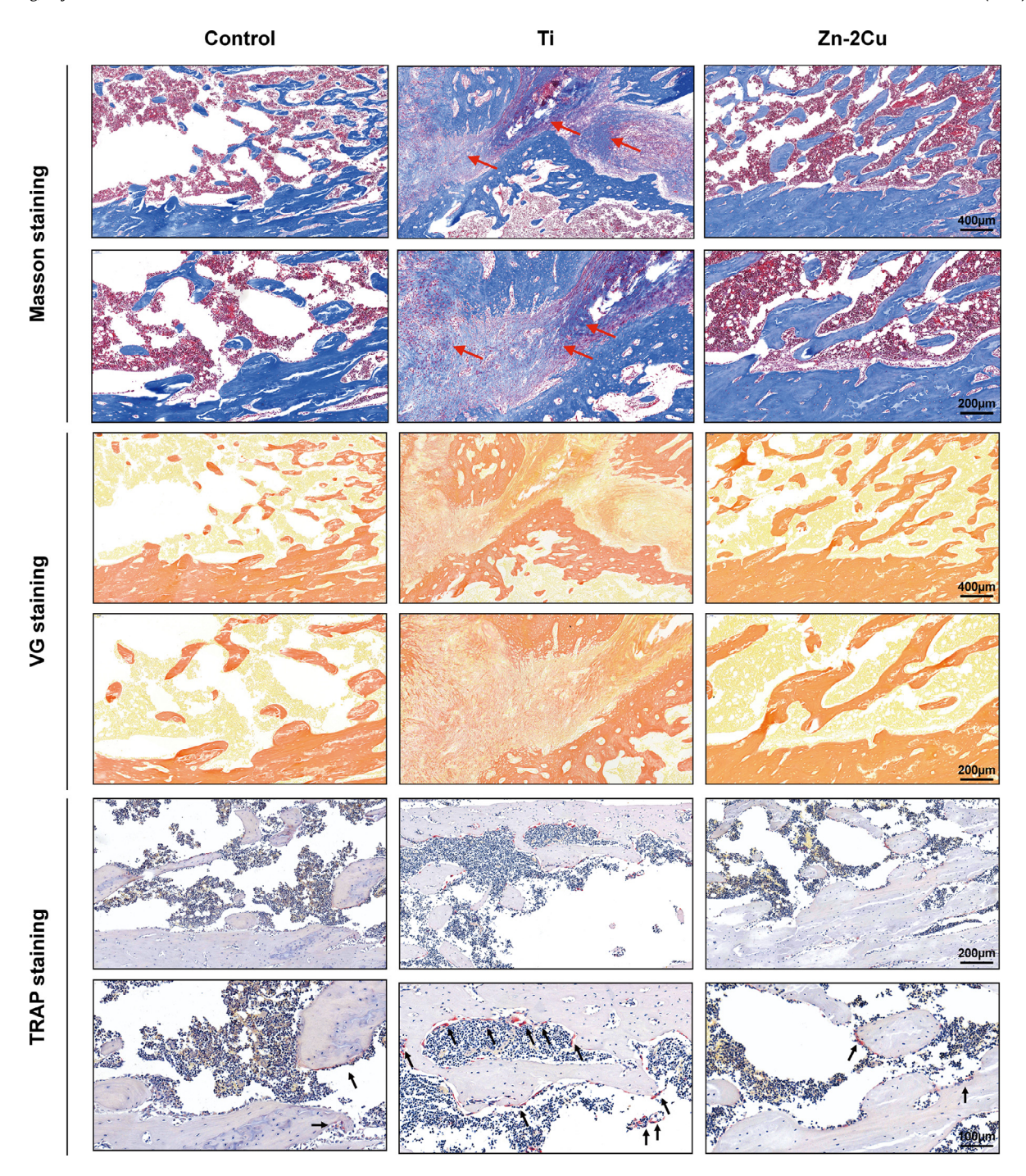


Fig. 9. Masson, Van Gieson (VG). and TRAP staining of longitudinal sections of the rat femoral medullary cavity at 6 weeks after implantation of Ti and Zn–2Cu intramedullary nails. Red and black arrows indicate immature bone and osteoclastic bone resorption, respectively. (For interpretation of the references to color in this figure legend, the reader is referred to the web version of this article.)

bilizing the biofilm structure in mature bacterial biofilms [87]. A major reason for the formation of MRSA bacterial biofilms is the creation of a suitable living environment for companion bacteria by the autolytic sacrifice of some MRSA bacteria, thereby providing a basis for biofilm formation. Various autolytic enzymes (especially peptidoglycan hydrolases) are involved in autolysis. The expression of autolysis associated genes including lytM, lytR, ArlR, and ArlS was inhibited remarkably, indicating another mechanism in the disruption of biofilm formation by the Zn–2Cu alloy [88,89]. In MRSA pathogenesis, clinical symptoms are severe due to the secretion of bacterial virulence factors. We found that the bacterial virulence-associated genes including empbp and ssaA were signifi-

cantly downregulated by the Zn–2Cu alloy, suggesting that the genetic virulence of MRSA was weakened remarkably.

Infection-related inflammatory toxic side-effects and bone loss are the most common clinical manifestations after bone infection. The inflammatory toxic side-effects often manifest as local inflammatory reactions, elevated blood inflammation indicators, and even symptoms of systemic infection. The *in vivo* study revealed stable body temperature of animals, and similar results of inflammatory indicators between the Zn-2Cu alloy and control groups. Additionally, HE staining showed less local inflammatory cells, indicating that the Zn-2Cu alloy was capable of preventing infection-related inflammatory toxic side-effects. Further, infection-related bone loss

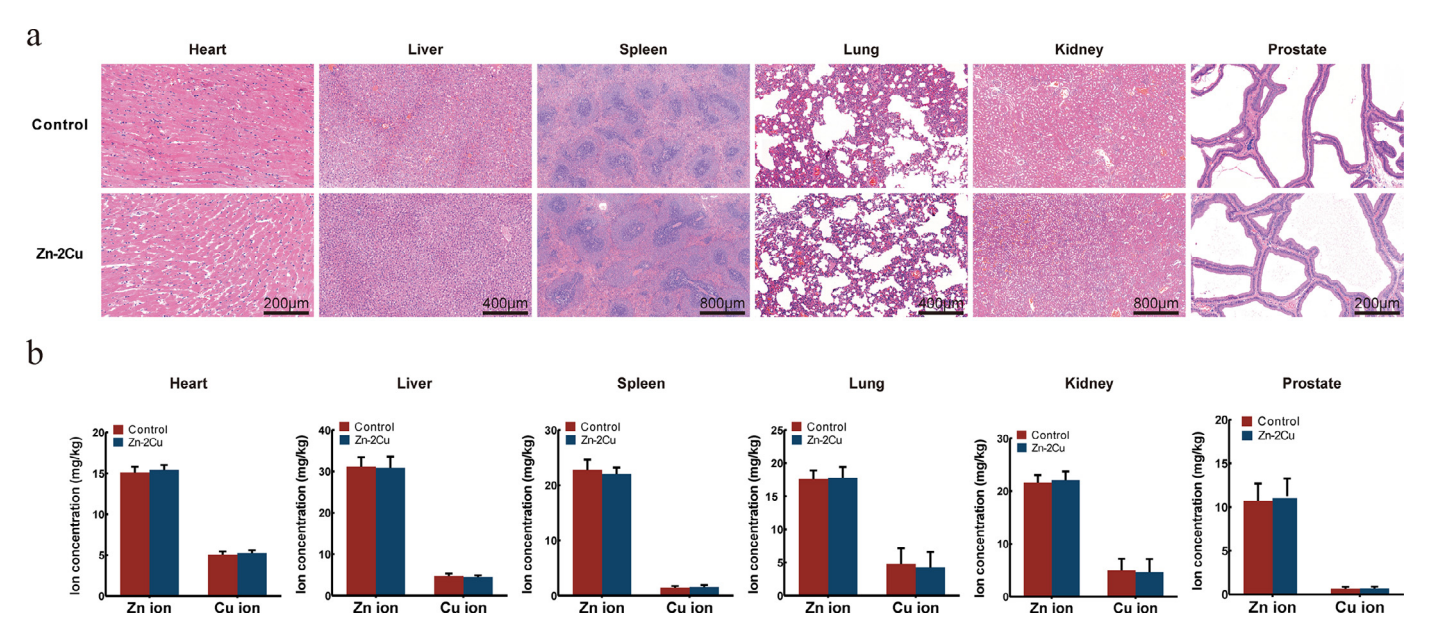


Fig. 10. (a) Hematoxylin-eosin (HE) staining of longitudinal pathological sections of and (b) Zn ion and Cu ion concentrations in the heart, liver, spleen, lung, kidney, and prostate of the healthy controls and animals implanted with Zn-2Cu alloy nails. Mean \pm SD, * p < 0.05; ** p < 0.01.

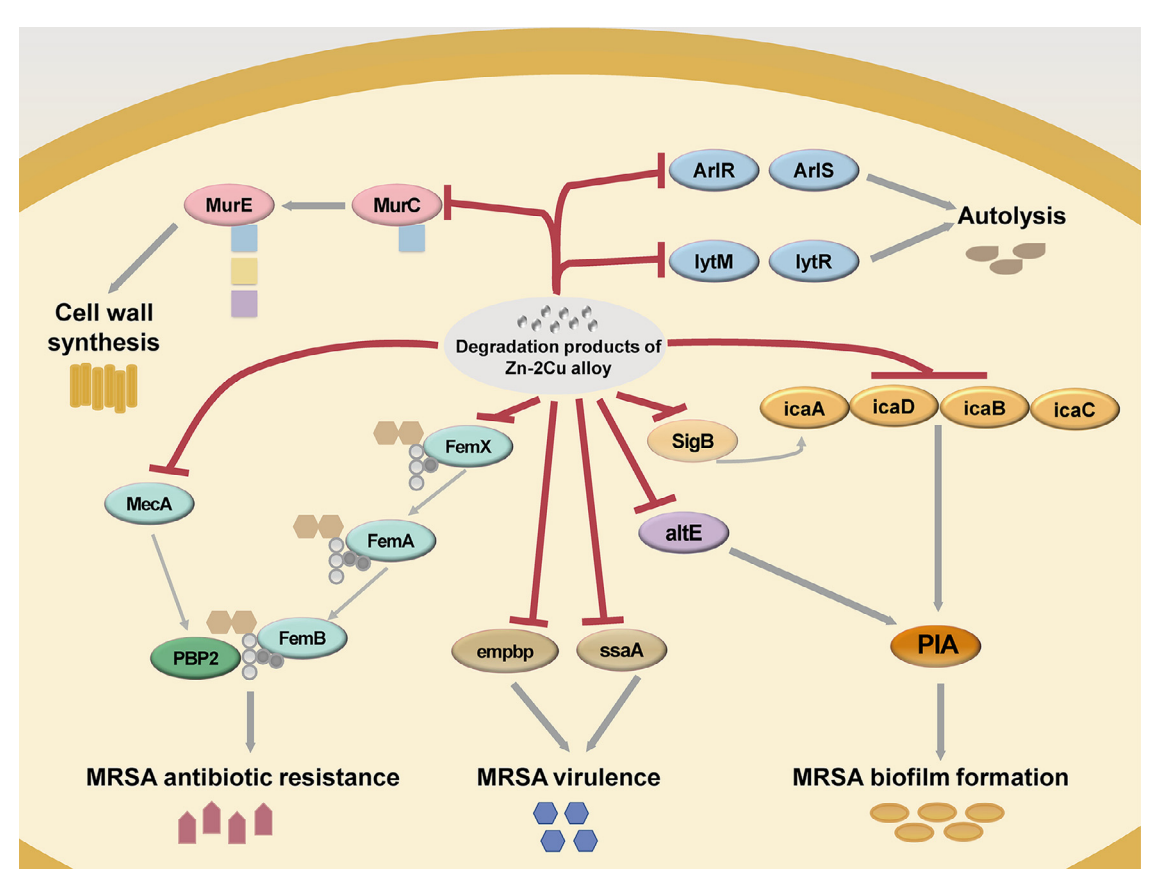


Fig. 11. The proposed mechanism underlying the Zn-2Cu alloy anti-microbial properties against MRSA.

is a knotty complication associated with orthopedic implant infection, which can activate osteoclasts and trigger the process of local bone loss. Compared to the control group, Masson and VG staining showed more immature bone formation (usually sequestrum) in the Ti group, whereas more mature new bone and bone mass was found in the Zn-2Cu alloy group. TRAP staining indicated massive osteoclast-induced bone resorption in the Ti group. In contrast,

little osteoclastogenesis was observed in the control group and Zn-2Cu alloy group. All these results proved the beneficial role of Zn-2Cu alloy in preventing infection-related bone loss.

Moreover, we found improved cytocompatibility and osteogenesis for Zn-2Cu alloy, the phenomenon that ZnCu alloy promotes osteogenesis may be related to the release of Cu ions. At present, there have been a large number of literature reports on

the mechanism of Cu ions promoting osteogenic differentiation. For instance, it has been demonstrated that an addition of 5% Cu into pure Ti contribute to good cytocompatibility [90]. And TiCu alloy did not negatively affect the adhesion, proliferation and apoptosis of osteoblasts. In contrast, it could increase the expression of osteogenesis-related gene including ALP, Collagen I, osteopontin and osteocalcin. Next, copper-containing stainless steel is also found it has improved cytocompatibility and increase the expression of osteogenic related genes through the Akt signaling pathway [91,92]. Besides, Jiang et al. found that graphene oxidecopper nanocomposites (GO-Cu) could improve the adhesion and osteogenic differentiation of rat bone marrow stem cells (BMSCs) [93]. Then, they proved that GO-Cu nanocomposites upregulate the expression of Hif-1 α in BMSCs by activating the Erk1/2 signaling pathway. Therefore, the sustained release of Cu ions from the Zn-2Cu alloy might be an important reason for this interesting phenomenon.

Therefore, biodegradable Zn-Cu alloys with satisfactory bactericidal properties can be manufactured into implants designed for a variety of clinical applications, including screws, intramedullary nails for fracture fixation or absorbable interference screws for sports medicine.

5. Conclusions

In this study, we carried out systematic characterizations by combining *in vitro* and *in vivo* studies to examine the antibacterial performance of Zn-Cu alloys. The Zn-2Cu alloy possessed desirable mechanical properties, satisfying biocompatibility, and favorable osteogenic properties. More importantly, the Zn-2Cu alloy showed strong antibacterial efficacy against both coagulase-positive and coagulase-negative staphylococci by preventing bacterial adhesion and biofilm formation. Additionally, the Zn-2Cu alloy eliminated MRSA infection and reduced its inflammatory toxic side-effects *in vivo*. PCR revealed that Zn-2Cu alloy downregulated the expression of genes related to wall synthesis, adhesion, colonization, biofilm formation, autolysis, and secretion of virulence factors in MRSA. Thus, biodegradable Zn-2Cu alloy is envisioned to be suitable for various orthopedic antibacterial implants and devices.

Declaration of Competing Interest

The authors declare that they have no known competing financial interests or personal relationships that could have appeared to influence the work reported in this paper.

Acknowledgments

This work was supported by National Natural Science Foundation of China [grant numbers 51931001, 51631009, 51431002, 51871004], NSFC/RGC Joint Research Scheme [grant number 51661165014], and Shanghai "Rising Stars of Medical Talent" Youth Development Program (Youth Medical Talents - Specialist Program). Xinhua Qu, Hongtao Yang, and Bo Jia contributed equally to this study.

Supplementary materials

Supplementary material associated with this article can be found, in the online version, at doi:10.1016/j.actbio.2020.09.041.

References

[1] A. Hogan, V.G. Heppert, A.J. Suda, Osteomyelitis, Arch. Orthop. Trauma Surg. 133 (9) (2013) 1183–1196. [2] P. Doshi, H. Gopalan, S. Sprague, C. Pradhan, S. Kulkarni, M. Bhandari, Incidence of infection following internal fixation of open and closed tibia fractures in India (INFINITI): a multi-centre observational cohort study, BMC Musculoskelet. Disord. 18 (1) (2017) 156.

- [3] H. Wang, H. Pei, M. Chen, H. Wang, Incidence and predictors of surgical site infection after ORIF in calcaneus fractures, a retrospective cohort study, J. Orthop. Surg. Res. 13 (1) (2018) 293.
- [4] N.T. Spina, I.S. Aleem, A. Nassr, B.D. Lawrence, Surgical site infections in spine surgery: preoperative prevention strategies to minimize risk, Glob. Spine J. 8 (4 Suppl) (2018) 31S–36S.
- [5] M. Wouthuyzen-Bakker, M. Sebillotte, J. Lomas, B. Kendrick, E.B. Palomares, O. Murillo, J. Parvizi, N. Shohat, J.C. Reinoso, R.E. Sanchez, M. Fernandez-Sampedro, E. Senneville, K. Huotari, J.M.B. Allende, A.B. Garcia, J. Lora-Tamayo, M.C. Ferrari, D. Vaznaisiene, E. Yusuf, C. Aboltins, R. Trebse, M.J. Salles, N. Benito, A. Vila, M.D.D. Toro, T.S. Kramer, S. Petersdorf, V. Diaz-Brito, Z.K. Tufan, M. Sanchez, C. Arvieux, A. Soriano, ESCMID Study Group for Implant-Associated Infections (ESGIAI), Timing of implant-removal in late acute periprosthetic joint infection: a multicenter observational study, J. Infect. 79 (3) (2019) 199–205.
- [6] J.M. Schierholz, J. Beuth, Implant infections: a haven for opportunistic bacteria, J. Hosp. Infect. 49 (2) (2001) 87–93.
- 7] D.P. Lew, F.A. Waldvogel, Osteomyelitis, Lancet 364 (9431) (2004) 369–379.
- [8] W. Costerton, R. Veeh, M. Shirtliff, M. Pasmore, C. Post, G. Ehrlich, The application of biofilm science to the study and control of chronic bacterial infections, J. Clin. Investig. 112 (10) (2003) 1466–1477.
- [9] S.J. Peacock, G.K. Paterson, Mechanisms of methicillin resistance in staphylococcus aureus, Ann. Rev. Biochem. 84 (2015) 577–601.
- [10] Y. Li, L. Liu, P. Wan, Z. Zhai, Z. Mao, Z. Ouyang, D. Yu, Q. Sun, L. Tan, L. Ren, Z. Zhu, Y. Hao, X. Qu, K. Yang, K. Dai, Biodegradable Mg-Cu alloy implants with antibacterial activity for the treatment of osteomyelitis: In vitro and in vivo evaluations, Biomaterials 106 (2016) 250–263.
- [11] Y. Li, G. Liu, Z. Zhai, L. Liu, H. Li, K. Yang, L. Tan, P. Wan, X. Liu, Z. Ouyang, Z. Yu, T. Tang, Z. Zhu, X. Qu, K. Dai, Antibacterial properties of magnesium in vitro and in an in vivo model of implant-associated methicillin-resistant staphylococcus aureus infection, Antimicrob. Agents Chemother. 58 (12) (2014) 7586-7591.
- [12] C. Liu, X. Fu, H. Pan, P. Wan, L. Wang, L. Tan, K. Wang, Y. Zhao, K. Yang, P.K. Chu, Biodegradable Mg-Cu alloys with enhanced osteogenesis, angiogenesis, and long-lasting antibacterial effects, Sci. Rep. 6 (2016) 27374.
- [13] Y.H. Zou, W. Jian, L.Y. Cui, R.C. Zeng, Q.Z. Wang, Q.X. Han, J. Qiu, X.B. Chen, D.C. Chen, S.K. Guan, Y.F. Zheng, Corrosion resistance and antibacterial activity of zinc-loaded montmorillonite coatings on biodegradable magnesium alloy AZ31, Acta biomater. (2019).
- [14] P. Tian, D. Xu, X. Liu, Mussel-inspired functionalization of PEO/PCL composite coating on a biodegradable AZ31 magnesium alloy, Colloids Surf. B Biointerfaces 141 (2016) 327–337.
- [15] L.-Y. Cui, P.-H. Qin, X.-L. Huang, Z.-Z. Yin, R.-C. Zeng, S.-Q. Li, E.-H. Han, Z.-L. Wang, Electrodeposition of TiO 2 layer-by-layer assembled composite coating and silane treatment on Mg alloy for corrosion resistance, Surf. Coat. Technol. 324 (2017) 560–568.
- [16] R.-C. Zeng, L.-J. Liu, K.-J. Luo, L. Shen, F. Zhang, S.-Q. Li, Y.-H. Zou, vitro corrosion and antibacterial properties of layer-by-layer assembled GS/PSS coating on AZ31 magnesium alloys, Trans. Nonferrous Metals Soc. China 25 (12) (2015) 4028–4039.
- [17] Y. Chen, W. Zhang, M.F. Maitz, M. Chen, H. Zhang, J. Mao, Y. Zhao, N. Huang, G. Wan, Comparative corrosion behavior of Zn with Fe and Mg in the course of immersion degradation in phosphate buffered saline, Corros. Sci. 111 (2016) 541–555
- [18] P.K. Bowen, J. Drelich, J. Goldman, Zinc exhibits ideal physiological corrosion behavior for bioabsorbable stents, Adv. Mater. 25 (18) (2013) 2577–2582.
- [19] H. Yang, X. Qu, W. Lin, C. Wang, D. Zhu, K. Dai, Y. Zheng, In vitro and in vivo studies on zinc-hydroxyapatite composites as novel biodegradable metal matrix composite for orthopedic applications, Acta Biomater. 71 (2018) 200–214.
- [20] H. Yang, X. Qu, W. Lin, D. Chen, D. Zhu, K. Dai, Y. Zheng, Enhanced osseointe-gration of Zn-Mg composites by tuning the release of Zn ions with sacrificial Mg-rich anode design, ACS Biomater. Sci. Eng. 5 (2) (2018) 453–467.
- [21] H. Yang, C. Wang, C. Liu, H. Chen, Y. Wu, J. Han, Z. Jia, W. Lin, D. Zhang, W. Li, Evolution of the degradation mechanism of pure zinc stent in the one-year study of rabbit abdominal aorta model, Biomaterials 145 (2017) 92–105.
- [22] H. Yang, B. Jia, Z. Zhang, X. Qu, G. Li, W. Lin, D. Zhu, K. Dai, Y. Zheng, Alloying design of biodegradable zinc as promising bone implants for load-bearing applications, Nat. Commun. 11 (1) (2020) 1–16.
- [23] Z. Tang, J. Niu, H. Huang, H. Zhang, J. Pei, J. Ou, G. Yuan, Potential biodegradable Zn-Cu binary alloys developed for cardiovascular implant applications, J. Mech. Behav. Biomed. Mater. 72 (2017) 182–191.
- [24] M. Li, Z. Ma, Y. Zhu, H. Xia, M. Yao, X. Chu, X. Wang, K. Yang, M. Yang, Y. Zhang, Toward a molecular understanding of the antibacterial mechanism of copper-bearing titanium alloys against staphylococcus aureus, Adv. Healthc. Mater. 5 (5) (2016) 557–566.
- [25] S. Ferraris, S. Spriano, Antibacterial titanium surfaces for medical implants, Mater. Sci. Eng. C-Mater. Biol. Appl. 61 (2016) 965–978.
- [26] J.E. Weder, C.T. Dillon, T.W. Hambley, B.J. Kennedy, P.A. Lay, J.R. Biffin, H.L. Regtop, N.M. Davies, Copper complexes of non-steroidal anti-inflammatory drugs: an opportunity yet to be realized, Coord. Chem. Rev. 232 (1-2) (2002) 95–126.
- [27] R. Liu, K. Memarzadeh, B. Chang, Y. Zhang, Z. Ma, R.P. Allaker, L. Ren, K. Yang,

Antibacterial effect of copper-bearing titanium alloy (Ti-Cu) against streptococcus mutans and porphyromonas gingivalis, Sci. Rep. 6 (2016) 29985.

- [28] R. Liu, Y. Tang, L. Zeng, Y. Zhao, Z. Ma, Z. Sun, L. Xiang, L. Ren, K. Yang, In vitro and in vivo studies of anti-bacterial copper-bearing titanium alloy for dental application, Dent. Mater.: off. Publ. Acad. Dent. Mater. 34 (8) (2018) 1112–1126.
- [29] D. Sun, D. Xu, C. Yang, J. Chen, M.B. Shahzad, Z. Sun, J. Zhao, T. Gu, K. Yang, G. Wang, Inhibition of Staphylococcus aureus biofilm by a copper-bearing 317L-Cu stainless steel and its corrosion resistance, Mater. Sci. Eng.. C, Mater. Biol. Appl. 69 (2016) 744–750.
- [30] D. Sun, D. Xu, C. Yang, M.B. Shahzad, Z. Sun, J. Xia, J. Zhao, T. Gu, K. Yang, G. Wang, An investigation of the antibacterial ability and cytotoxicity of a novel cu-bearing 317L stainless steel, Sci. Rep. 6 (2016) 29244.
- [31] D. Zhang, L. Ren, Y. Zhang, N. Xue, K. Yang, M. Zhong, Antibacterial activity against Porphyromonas gingivalis and biological characteristics of antibacterial stainless steel, Colloids Surf. B Biointerfaces 105 (2013) 51–57.
- [32] S. Guo, Y. Lu, S. Wu, L. Liu, M. He, C. Zhao, Y. Gan, J. Lin, J. Luo, X. Xu, J. Lin, Preliminary study on the corrosion resistance, antibacterial activity and cytotoxicity of selective-laser-melted Ti6Al4V-xCu alloys, Mater. Sci. Eng. C, Mater. Biol. Appl. 72 (2017) 631–640.
- [33] R. Liu, K. Memarzadeh, B. Chang, Y. Zhang, Z. Ma, R.P. Allaker, L. Ren, K. Yang, Antibacterial effect of copper-bearing titanium alloy (Ti-Cu) against streptococcus mutans and porphyromonas gingivalis, Sci. Rep. 6 (2016) 29985.
- [34] Z. Ma, M. Li, R. Liu, L. Ren, Y. Zhang, H. Pan, Y. Zhao, K. Yang, In vitro study on an antibacterial Ti-5Cu alloy for medical application, J. Mater. Sci. Mater. Med. 27 (5) (2016) 91.
- [35] X. Tong, Z. Shi, L. Xu, J. Lin, D. Zhang, K. Wang, Y. Li, C. Wen, Degradation behavior, cytotoxicity, hemolysis, and antibacterial properties of electro-deposited Zn-Cu metal foams as potential biodegradable bone implants, Acta Biomater. 102 (2020) 481–492.
- [36] C.K. Nijjar, M.H. Smith, I.J. Eltringham, Adjunctive mecA PCR for routine detection of methicillin susceptibility in clinical isolates of coagulase-negative staphylococci, J. Clin. Microbiol. 52 (5) (2014) 1678–1681.
- [37] J. Wang, F. Witte, T. Xi, Y. Zheng, K. Yang, Y. Yang, D. Zhao, J. Meng, Y. Li, W. Li, K. Chan, L. Qin, Recommendation for modifying current cytotoxicity testing standards for biodegradable magnesium-based materials, Acta Biomater. 21 (2015) 237–249.
- [38] E. ISO, 10993-5Biological Evaluation of Medical Devices. Part 5: Tests for In Vitro Cytotoxicity, International Organization for Standardization, Geneva, Switzerland, 2009.
- [39] A.F. Cipriano, J. Lin, A. Lin, A. Sallee, B. Le, M.C. Cortez Alcaraz, R.G. Guan, G. Botimer, S. Inceoglu, H. Liu, Degradation of bioresorbable Mg-4Zn-1Sr intramedullary pins and associated biological responses in vitro and in vivo, ACS Appl. Mater. Interfaces 9 (51) (2017) 44332-44355.
- [40] P. Han, P. Cheng, S. Zhang, C. Zhao, J. Ni, Y. Zhang, W. Zhong, P. Hou, X. Zhang, Y. Zheng, Y. Chai, In vitro and in vivo studies on the degradation of high-purity Mg (99.99wt.%) screw with femoral intracondylar fractured rabbit model, Biomaterials 64 (2015) 57–69.
- [41] J.W. Lee, H.S. Han, K.J. Han, J. Park, H. Jeon, M.R. Ok, H.K. Seok, J.P. Ahn, K.E. Lee, D.H. Lee, S.J. Yang, S.Y. Cho, P.R. Cha, H. Kwon, T.H. Nam, J.H. Han, H.J. Rho, K.S. Lee, Y.C. Kim, D. Mantovani, Long-term clinical study and multiscale analysis of in vivo biodegradation mechanism of Mg alloy, Proc. Natl. Acad. Sci. U S A 113 (3) (2016) 716–721.
- [42] E. Willbold, X. Gu, D. Albert, K. Kalla, K. Bobe, M. Brauneis, C. Janning, J. Nellesen, W. Czayka, W. Tillmann, Y. Zheng, F. Witte, Effect of the addition of low rare earth elements (lanthanum, neodymium, cerium) on the biodegradation and biocompatibility of magnesium, Acta Biomater. 11 (2015) 554–562.
- [43] F. Witte, V. Kaese, H. Haferkamp, E. Switzer, A. Meyer-Lindenberg, C.J. Wirth, H. Windhagen, In vivo corrosion of four magnesium alloys and the associated bone response, Biomaterials 26 (17) (2005) 3557–3563.
- [44] D. Zhao, S. Huang, F. Lu, B. Wang, L. Yang, L. Qin, K. Yang, Y. Li, W. Li, W. Wang, S. Tian, X. Zhang, W. Gao, Z. Wang, Y. Zhang, X. Xie, J. Wang, J. Li, Vascularized bone grafting fixed by biodegradable magnesium screw for treating osteonecrosis of the femoral head, Biomaterials 81 (2016) 84–92.
- [45] D. Zhao, F. Witte, F. Lu, J. Wang, J. Li, L. Qin, Current status on clinical applications of magnesium-based orthopaedic implants: a review from clinical translational perspective, Biomaterials 112 (2017) 287–302.
- [46] X.N. Gu, X.H. Xie, N. Li, Y.F. Zheng, L. Qin, In vitro and in vivo studies on a Mg-Sr binary alloy system developed as a new kind of biodegradable metal, Acta Biomater. 8 (6) (2012) 2360–2374.
- [47] K. Jahn, H. Saito, H. Taipaleenmaki, A. Gasser, N. Hort, F. Feyerabend, H. Schluter, J.M. Rueger, W. Lehmann, R. Willumeit-Romer, E. Hesse, Intramedullary Mg2Ag nails augment callus formation during fracture healing in mice, Acta Biomater. 36 (2016) 350–360.
- [48] D. Dziuba, A. Meyer-Lindenberg, J.M. Seitz, H. Waizy, N. Angrisani, J. Reifenrath, Long-term in vivo degradation behaviour and biocompatibility of the magnesium alloy ZEK100 for use as a biodegradable bone implant, Acta Biomater. 9 (10) (2013) 8548–8560.
- [49] C. Rossig, N. Angrisani, P. Helmecke, S. Besdo, J.M. Seitz, B. Welke, N. Fedchenko, H. Kock, J. Reifenrath, In vivo evaluation of a magnesium-based degradable intramedullary nailing system in a sheep model, Acta Biomater. 25 (2015) 369–383.
- [50] H. Windhagen, K. Radtke, A. Weizbauer, J. Diekmann, Y. Noll, U. Kreimeyer, R. Schavan, C. Stukenborg-Colsman, H. Waizy, Biodegradable magnesium-based screw clinically equivalent to titanium screw in hallux valgus surgery: short term results of the first prospective, randomized, controlled clinical pilot study, Biomed. Eng. Online 12 (2013) 62.

[51] A. Chaya, S. Yoshizawa, K. Verdelis, N. Myers, B.J. Costello, D.T. Chou, S. Pal, S. Maiti, P.N. Kumta, C. Sfeir, In vivo study of magnesium plate and screw degradation and bone fracture healing, Acta Biomater. 18 (2015) 262–269.

- [52] D. Tie, R. Guan, H. Liu, A. Cipriano, Y. Liu, Q. Wang, Y. Huang, N. Hort, An in vivo study on the metabolism and osteogenic activity of bioabsorbable Mg-1Sr alloy, Acta Biomater. 29 (2016) 455–467.
- [53] S.E. Henderson, K. Verdelis, S. Maiti, S. Pal, W.L. Chung, D.T. Chou, P.N. Kumta, A.J. Almarza, Magnesium alloys as a biomaterial for degradable craniofacial screws, Acta Biomater 10 (5) (2014) 2323–2332.
- [54] D. Chen, Y. He, H. Tao, Y. Zhang, Y. Jiang, X. Zhang, S. Zhang, Biocompatibility of magnesium-zinc alloy in biodegradable orthopedic implants, Int. J. Mol. Med. 28 (3) (2011) 343–348.
- [55] E. Zhang, L. Xu, G. Yu, F. Pan, K. Yang, In vivo evaluation of biodegradable magnesium alloy bone implant in the first 6 months implantation, J. Biomed. Mater. Res. A 90 (3) (2009) 882–893.
- [56] X. Guan, M. Xiong, F. Zeng, B. Xu, L. Yang, H. Guo, J. Niu, J. Zhang, C. Chen, J. Pei, H. Huang, G. Yuan, Enhancement of osteogenesis and biodegradation control by brushite coating on Mg-Nd-Zn-Zr alloy for mandibular bone repair, ACS Appl. Mater. Interfaces 6 (23) (2014) 21525–21533.
- [57] X. Zhang, G. Yuan, J. Niu, P. Fu, W. Ding, Microstructure, mechanical properties, biocorrosion behavior, and cytotoxicity of as-extruded Mg-Nd-Zn-Zr alloy with different extrusion ratios, J. Mech. Behav. Biomed. Mater. 9 (2012) 153–162.
- [58] N. Erdmann, N. Angrisani, J. Reifenrath, A. Lucas, F. Thorey, D. Bormann, A. Meyer-Lindenberg, Biomechanical testing and degradation analysis of MgCa0.8 alloy screws: a comparative in vivo study in rabbits, Acta Biomater. 7 (3) (2011) 1421–1428.
- [59] L. Tan, Q. Wang, X. Lin, P. Wan, G. Zhang, Q. Zhang, K. Yang, Loss of mechanical properties in vivo and bone-implant interface strength of AZ31B magnesium alloy screws with Si-containing coating, Acta Biomater. 10 (5) (2014) 2333–2340.
- [60] Z. Li, X. Gu, S. Lou, Y. Zheng, The development of binary Mg-Ca alloys for use as biodegradable materials within bone, Biomaterials 29 (10) (2008) 1329–1344.
- [61] H.M. Wong, Y. Zhao, V. Tam, S. Wu, P.K. Chu, Y. Zheng, M.K. To, F.K. Leung, K.D. Luk, K.M. Cheung, K.W. Yeung, In vivo stimulation of bone formation by aluminum and oxygen plasma surface-modified magnesium implants, Biomaterials 34 (38) (2013) 9863–9876.
- [62] P. Xiong, J. Yan, P. Wang, Z. Jia, W. Zhou, W. Yuan, Y. Li, Y. Liu, Y. Cheng, D. Chen, Y. Zheng, A pH-sensitive self-healing coating for biodegradable magnesium implants, Acta Biomater. (2019).
- [63] Y. Qin, P. Wen, H. Guo, D. Xia, Y. Zheng, L. Jauer, R. Poprawe, M. Voshage, J.H. Schleifenbaum, Additive manufacturing of biodegradable metals: current research status and future perspectives, Acta Biomater. (2019).
- [64] J. Liu, Y. Lin, D. Bian, M. Wang, Z. Lin, X. Chu, W. Li, Y. Liu, Z. Shen, Y. Liu, Y. Tong, Z. Xu, Y. Zhang, Y. Zheng, In vitro and in vivo studies of Mg-30Sc alloys with different phase structure for potential usage within bone, Acta Biomater. (2019)
- [65] L.Y. Li, L.Y. Cui, R.C. Zeng, S.Q. Li, X.B. Chen, Y. Zheng, M.B. Kannan, Advances in functionalized polymer coatings on biodegradable magnesium alloys - a review, Acta Biomater. 79 (2018) 23–36.
- [66] Y. Liu, Y. Wu, D. Bian, S. Gao, S. Leeflang, H. Guo, Y. Zheng, J. Zhou, Study on the Mg-Li-Zn ternary alloy system with improved mechanical properties, good degradation performance and different responses to cells, Acta Biomater. 62 (2017) 418–433.
- [67] J.W. Lee, H.S. Han, K.J. Han, J. Park, H. Jeon, M.R. Ok, H.K. Seok, J.P. Ahn, K.E. Lee, D.H. Lee, Long-term clinical study and multiscale analysis of in vivo biodegradation mechanism of Mg alloy, Proceed. Natl. Acad. Sci. United States Am. 113 (3) (2016).
- [68] Y. Li, L. Liu, P. Wan, Z. Zhai, Z. Mao, Z. Ouyang, D. Yu, Q. Sun, L. Tan, L. Ren, Biodegradable Mg-Cu alloy implants with antibacterial activity for the treatment of osteomyelitis: in vitro and in vivo evaluations, Biomaterials 106 (2016) 250, 262
- [69] H. Yang, X. Qu, W. Lin, C. Wang, D. Zhu, K. Dai, Y. Zheng, In vitro and in vivo studies on zinc-hydroxyapatite composites as novel biodegradable metal matrix composite for orthopedic applications, Acta Biomater. (2018).
- [70] H. Yang, X. Qu, W. Lin, D. Chen, D. Zhu, K. Dai, Y.J.A.B.S. Zheng, Engineering, enhanced osseointegration of Zn-Mg composites by tuning the release of Zn ions with sacrificial Mg rich anode design, (2018).
- [71] H. Li, H. Yang, Y. Zheng, F. Zhou, K. Qiu, X. Wang, Design and characterizations of novel biodegradable ternary Zn-based alloys with IIA nutrient alloying elements Mg, Ca and Sr, Mater. Des. 83 (2015) 95–102.
- [72] B. Jia, H. Yang, Y. Han, Z. Zhang, X. Qu, Y. Zhuang, Q. Wu, Y. Zheng, K. Dai, In vitro and in vivo studies of Zn-Mn biodegradable metals designed for orthopedic applications, Acta Biomater. (2020).
- [73] G. Li, H. Yang, Y. Zheng, X.-H. Chen, J.-A. Yang, D. Zhu, L. Ruan, K. Takashima, Challenges in the use of zinc and its alloys as biodegradable metals: perspective from biomechanical compatibility, Acta Biomater. (2019).
- [74] J. Lin, X. Tong, Z. Shi, D. Zhang, L. Zhang, K. Wang, A. Wei, L. Jin, J. Lin, Y. Li, C. Wen, A biodegradable Zn-1Cu-0.1Ti alloy with antibacterial properties for orthopedic applications, Acta Biomater. 106 (2020) 410-427.
- [75] X. Tong, Z. Shi, L. Xu, J. Lin, D. Zhang, K. Wang, Y. Li, C. Wen, Degradation behavior, cytotoxicity, hemolysis, and antibacterial properties of electro-deposited Zn-Cu metal foams as potential biodegradable bone implants, Acta Biomater. 102 (2020) 481–492.
- [76] K.S. Alathel, N. Marraiki, A.F.M. Arif, S.S. Akhtar, J. Mostaghimi, M. Ibrahim,

X. Qu, H. Yang, B. Jia et al.

- Effect of Ni and Zn elements on the microstructure and antibacterial properties of Cu coatings, J. Eng. Mater. Technol.Trans. Asme 142 (1) (2020).
- [77] Z. Tang, J. Niu, H. Huang, H. Zhang, J. Pei, J. Ou, G. Yuan, Potential biodegradable Zn-Cu binary alloys developed for cardiovascular implant applications, J. Mech. Behav. Biomed. Mater. 72 (2017) 182–191.
- [78] M. Sova, A. Kovac, S. Turk, M. Hrast, D. Blanot, S. Gobec, Phosphorylated hydroxyethylamines as novel inhibitors of the bacterial cell wall biosynthesis enzymes MurC to MurF, Bioorg. Chem. 37 (6) (2009) 217–222.
- [79] C.R. Arciola, D. Campoccia, L. Montanaro, Implant infections: adhesion, biofilm formation and immune evasion, Nat. Rev. Microbiol. 16 (7) (2018) 397–409.
- [80] S. Zhang, H. Tang, Y. Wang, B. Nie, H. Yang, W. Yuan, X. Qu, B. Yue, Antibacterial and antibiofilm effects of flufenamic acid against methicillin-resistant staphylococcus aureus, Pharmacol. Res. 160 (2020) 105067.
- [81] J. Li, D. Zhai, F. Lv, Q. Yu, H. Ma, J. Yin, Z. Yi, M. Liu, J. Chang, C. Wu, Preparation of copper-containing bioactive glass/eggshell membrane nanocomposites for improving angiogenesis, antibacterial activity and wound healing, Acta Biomater. 36 (2016) 254–266.
- [82] N.K. Archer, M.J. Mazaitis, J.W. Costerton, J.G. Leid, M.E. Powers, M.E. Shirtliff, Staphylococcus aureus biofilms: properties, regulation, and roles in human disease, Virulence 2 (5) (2011) 445–459.
- [83] B. Cui, P.M. Smooker, D.A. Rouch, M.A. Deighton, Effects of erythromycin on the phenotypic and genotypic biofilm expression in two clinical Staphylococcus capitis subspecies and a functional analysis of Ica proteins in S. capitis, J. Med. Microbiol. 64 (6) (2015) 591–604.
- [84] H. Rohde, S. Frankenberger, U. Zahringer, D. Mack, Structure, function and contribution of polysaccharide intercellular adhesin (PIA) to Staphylococcus epidermidis biofilm formation and pathogenesis of biomaterial-associated infections, Eur. J. Cell Biol. 89 (1) (2010) 103–111.
- [85] W.Y. Jeng, T.P. Ko, C.I. Liu, R.T. Guo, C.L. Liu, H.L. Shr, A.H. Wang, Crystal structure of IcaR, a repressor of the TetR family implicated in biofilm formation in Staphylococcus epidermidis, Nucleic. Acids Res. 36 (5) (2008) 1567–1577.

- [86] C. Cucarella, M.A. Tormo, C. Ubeda, M.P. Trotonda, M. Monzon, C. Peris, B. Amorena, I. Lasa, J.R. Penades, Role of biofilm-associated protein bap in the pathogenesis of bovine Staphylococcus aureus, Infect. Immun. 72 (4) (2004) 2177–2185.
- [87] M. Sabate Bresco, L.G. Harris, K. Thompson, B. Stanic, M. Morgenstern, L. O'Mahony, R.G. Richards, T.F. Moriarty, Pathogenic mechanisms and host interactions in staphylococcus epidermidis device-related infection, Front Microbiol. 8 (2017) 1401.
- [88] B.K. Sharma-Kuinkel, E.E. Mann, J.S. Ahn, L.J. Kuechenmeister, P.M. Dunman, K.W. Bayles, The Staphylococcus aureus LytSR two-component regulatory system affects biofilm formation, J. Bacteriol. 191 (15) (2009) 4767–4775.
- [89] X. Liang, L. Zheng, C. Landwehr, D. Lunsford, D. Holmes, Y. Ji, Global regulation of gene expression by ArIRS, a two-component signal transduction regulatory system of staphylococcus aureus. I. Bacteriol. 187 (15) (2005) 5486–5492.
- system of staphylococcus aureus, J. Bacteriol. 187 (15) (2005) 5486–5492. [90] R. Liu, Z. Ma, S. Kunle Kolawole, L. Zeng, Y. Zhao, L. Ren, K. Yang, In vitro study on cytocompatibility and osteogenesis ability of Ti-Cu alloy, J. Mater. Sci. Mater. Med. 30 (7) (2019) 75.
- [91] Y. Yuan, S. Jin, X. Qi, X. Chen, W. Zhang, K. Yang, H. Zhong, Osteogenesis stimulation by copper-containing 316L stainless steel via activation of akt cell signaling pathway and Runx2 upregulation, J. Mater. Sci. Technol. 35 (11) (2019) 2727–2733.
- [92] L. Ren, H.M. Wong, C.H. Yan, K.W. Yeung, K. Yang, Osteogenic ability of Cu-bearing stainless steel, J. Biomed. Mater. Res. B Appl. Biomater 103 (7) (2015) 1433–1444.
- [93] W. Zhang, Q. Chang, L. Xu, G. Li, G. Yang, X. Ding, X. Wang, D. Cui, X. Jiang, Graphene oxide-copper nanocomposite-coated porous CaP scaffold for vascularized bone regeneration via activation of hif-1alpha, Adv. Healthc. Mater. 5 (11) (2016) 1299–1309.